Clim Dyn
DOI 10.1007/s00382-011-1126-x

Comparison of tropical cyclogenesis indices on seasonal to interannual timescales

Christophe E. Menkes · Matthieu Lengaigne · Patrick Marchesiello · Nicolas C. Jourdain · Emmanuel M. Vincent · Jérôme Lefèvre · Fabrice Chauvin · Jean-Francois Royer

Received: 7 July 2010 / Accepted: 15 June 2011

Abstract This paper evaluates the performances of four cyclogenesis indices against observed tropical cyclone genesis on a global scale over the period 1979–2001. These indices are: the Genesis Potential Index; the Yearly Genesis Parameter; the Modified Yearly Convective Genesis Potential Index; and the Tippett et al. Index (J Clim, 2011), hereafter referred to as TCS. Choosing ERA40, NCEP2, NCEP or JRA25 reanalysis to calculate these indices can yield regional differences but overall does not change the main conclusions arising from this study. By contrast, differences between indices are large and vary depending on the regions and on the timescales considered. All indices except the TCS show an equatorward bias in mean cyclogenesis, especially in the northern hemisphere where this bias can reach 5°. Mean simulated genesis numbers for all indices exhibit large regional discrepancies, which can commonly reach up to ±50%. For the seasonal timescales on which the indices are historically fitted, performances also vary widely in terms of amplitude although in general they all reproduce the cyclogenesis seasonality adequately. At the seasonal scale, the TCS seems to be the best fitted index overall. The most striking feature at interannual scales is the inability of all indices to reproduce the observed cyclogenesis amplitude. The indices also lack the ability to reproduce the general interannual phase variability, but they do, however, acceptably reproduce the phase variability linked to El Niño/Southern Oscillation (ENSO)—a major driver of tropical cyclones interannual variations. In terms of cyclogenesis mechanisms that can be inferred from the analysis of the index terms, there are wide variations from one index to

C. E. Menkes · M. Lengaigne · E. M. Vincent
IRD, Laboratoire d'Océanographie et du Climat: Expérimentation et Approches Numériques (LOCEAN), IRD/UPMC/CNRS/MNHN, Paris, France

M. Lengaigne
e-mail: matthieu.lengaigne@ird.fr

E. M. Vincent
e-mail: emmanuel.vincent@locean-ipsl.upmc.fr

M. Lengaigne
IRD, National Institute of Oceanography, Goa, India

C. E. Menkes · N. C. Jourdain · J. Lefèvre
IRD, BP A5, Nouméa Cedex 98848, New Caledonia

N. C. Jourdain
e-mail: Nicolas.Jourdain@hmg.inpg.fr

J. Lefèvre
e-mail: jerome.lefevre@ird.fr

P. Marchesiello · J. Lefèvre
IRD, Laboratoire d'Etudes en Géophysique et Océanographie Spatiale (LEGOS), 14 Av Edouard Belin, 31400 Toulouse, France
e-mail: patrick.marchesiello@ird.fr

F. Chauvin · J.-F. Royer
Météo-France, CNRM/GAME (Météo-France/CNRS), 42, Avenue Coriolis, 31057 Toulouse Cedex 01, France
e-mail: fabrice.chauvin@meteo.fr

J.-F. Royer
e-mail: jean-francois.royer@meteo.fr

C. E. Menkes (✉)
LOCEAN, IRD/UPMC/MNHN/CNRS, Institut de Recherche Pour le Développement, BP A5 Boîte 100, 98848 Nouméa Cedex, New Caledonia
e-mail: christophe.menkes@ird.fr

another at seasonal and interannual timescales and caution is advised when using these terms from one index only. They do, however, show a very good coherence at ENSO scale thus inspiring confidence in the mechanism interpretations that can be obtained by the use of any index. Finally, part of the gap between the observed and simulated cyclogenesis amplitudes may be attributable to stochastic processes, which cannot be inferred from environmental indices that only represent a potential for cyclogenesis.

Keywords Cyclogenesis indices · Atmospheric reanalyses · ENSO · Cyclone stochasticity

1 Introduction

Understanding the generation, development and fate of tropical cyclones is a major challenge for scientists and is of great importance to society. Tropical cyclones occur in specific large-scale environments and to improve understanding of how that environment favours cyclogenesis, Gray (1968, 1975, 1979) first developed an empirical cyclogenesis index referred to as the Yearly Genesis Parameter (YGP). This first index was followed by the construction of two other well known indices: the Modified Yearly Convective Genesis Potential Index (CYGP) developed by Royer et al. (1998) which is a variant of the YGP, and the Genesis Potential Index (GPI) developed by Emanuel and Nolan (2004). Tippett et al. (2011) have recently proposed improvements to the GPI. These improvements are referred to as 'TCS' (Tippett, Camargo, Sobel) in this paper. The TCS allows a better representation of off-equatorial cyclogenesis maxima and of cyclogenesis during unfavourable seasons Murakami and Wang (2010) discuss another variant of the GPI for the western North Pacific and Emanuel (2010) has also proposed a more general modification of the GPI which has particular importance in relation to issues of climate change.

The advantages of these empirical indices are that they can be applied to observed or simulated low resolution datasets for the current climate (e.g. Gray 1979; Watterson et al. 1995; Camargo et al. 2007a, b; Royer et al. 1998; Tippett et al. 2011; Yokoi et al. 2009 etc.) and future climates (e.g. Caron and Jones 2008; Royer and Chauvin 2009; McDonald et al. 2005; Kim et al. 2010). They can also be used to study cyclogenesis frequencies on a number of timescales ranging from intraseasonal (Camargo et al. 2009) to interannual timescales (Camargo et al. 2007a, b; Watterson et al. 1995; Lyon and Camargo 2009; Vincent et al. 2009; Tippett et al. 2011). These indices may also inherently reveal the main large-scale factors influencing cyclogenesis on mean, seasonal or specific event levels, such as El Niño/Southern Oscillation (ENSO, Camargo et al. 2007a; Watterson et al. 1995; Chand and Walsh 2009; Vincent et al. 2009) or during the Madden Julian Oscillation (MJO, Camargo et al. 2009).

The four indices are all based on the same principle: that the large-scale environment favourable to cyclogenesis is a product of thermal and dynamical potential, which themselves are combinations of similar ingredients but with different formulations. It is important to stress that the formulations entering these indices are empirically fitted onto a global and seasonal scale designed to provide values as realistic as possible within these scales. Thus, the constants and the exact formulations by which the individual terms enter the final index can differ significantly from one index to the other. Furthermore, the indices represent a potential for cyclogenesis controlled by large scale climatic variations but do not take into account other processes important for actual tropical cyclones (TCs) generation such as stochastic processes (Simpson et al. 1997; Jourdain et al. 2010) or small-scale triggers (Gray 1998) which may lower the expected index performances on different scales (Camargo et al. 2009; Jourdain et al. 2010).

Another source of uncertainty in evaluating TC numbers from these indices arises from the climate datasets used for their calculation. For example, Kim et al. (2010) have used four different reanalyses, ERA40 (Uppala and Co-authors 2005), JRA25 (Onogi et al. 2007), NCEP1 (Kalnay et al. 1996) and NCEP2 (Kanamitsu et al. 2002) reanalyses to compare the CYGP performances on seasonal scales. They conclude that no particular reanalysis outperforms the others, although their individual performances can vary significantly from one region to another. A similar conclusion was reached by Tippett et al. (2011), using the TCS with ERA40 and NCEP1, and also by Camargo et al. (2009), using the GPI at the MJO scale where the ERA40 indices showed a higher variability due to larger mid-tropospheric humidity. Because the functional forms of terms entering the index formulation vary from one index to the other, it is not a priori obvious to translate the information from different studies into a clear message. Even when only one index were used, difficulties arose which compelled Kim et al. (2010) to conclude that "these results illustrate that ConvGP" (the CYGP) "identifies many aspects in seasonal TC genesis but with some deficiencies, indicating that it has both useful information and limitations".

However, there is still a need to understand how these four indices compare on different scales. When examining results from previously published work (Royer et al. 1998; Royer and Chauvin 2009; McDonald et al. 2005, for the YGP and CYGP, Camargo et al. 2007a, b for the GPI and Tippett et al. 2011 for the TCS), it appears that these indices give roughly similar geographical distributions and seasonal variability in most cyclogenesis regions. Additional quantitative comparisons between the YGP and CYGP have been described in

Caron and Jones (2008) who concluded that the CYGP is more appropriate than the YGP to study cyclogenesis in the context of global warming. Watterson et al. (1995) also concluded that the YGP is not an accurate index to grasp interannual variability of cyclogenesis in the Pacific Ocean. The CYGP also shows some biases: it globally underestimates cyclogenesis in the northern Hemisphere (e.g. McDonald et al. 2005; Kim et al. 2010) but so far it has not been evaluated in terms of its accuracy on interannual timescales. On the other hand, Camargo et al. (2007a, b) and Tippett et al. (2011) have explored the relationship between ENSO and the GPI/TCS response and show that the GPI and TCS have some skills in representing the phase relationship between ENSO and tropical cyclogenesis. However, they do not report the simulated TC genesis numbers on ENSO timescales, which creates difficulties in making comparisons between the YGP index types (YGP/CYGP) and the GPI types (GPI, TCS). Because individual terms entering the index may help to understand the main factors involved in cyclogenesis, Tippett et al. (2011) have explored the relative contribution of these components to cyclogenesis. Camargo et al. (2009) have investigated the role of these terms during MJOs and Camargo et al. (2007a) have described their evolution during ENSO. The latter study has shown that a combination of vorticity, relative humidity, and vertical wind shear can explain most of the GPI behaviour during ENSO. They have also demonstrated that the contribution of each term in the final index also has regional variations thus suggesting that different mechanisms may be at work (in reality) in different regions (Camargo and Sobel 2007).

Interannual variability can be high in many regions of the world, some (but not all) of which can be linked to ENSO (see Landsea 2000; Chu 2004 for reviews). Therefore, it is important to have a better understanding of how effective the indices are in simulating observed phase and amplitude of TC formation on interannual timescales. Whether the indices are in agreement and can bring coherent insights about the possible dynamics of TC formation through their contributing terms also needs to be investigated. The main purpose of this study is to understand and evaluate the common features of these four indices calculated with four reanalyses with regards to observations on seasonal and interannual scales and also to understand how the terms composing these indices contribute to cyclogenesis on these scales.

2 Data and cyclogenesis indices

2.1 Tropical cyclone, reanalyses data and indices

For the tropical cyclone genesis data, we use the global datasets gathered and kindly provided by Dr. Emanuel and freely available online at (ftp://texmex.mit.edu/pub/emanuel/HURR/tracks_netcdf/) which are derived from a compilation of the best track datasets from diverse centres. Because our interest lies in characterizing the performances of cyclogenesis indices, we define cyclogenesis location as the first position of a storm in the dataset, provided the storm reaches 17 m/s at some point along its trajectory; a definition identical to McDonald et al. (2005) and very similar to that of Watterson et al. (1995). The definition is somewhat arbitrary and may vary from study to study. For instance, other studies have defined cyclogenesis location as the first point in which a storm reaches 17 m/s (e.g. Caron and Jones 2008). The difference between the two definitions is illustrated in Fig. 1 which demonstrates that the latter distribution has a poleward offset of about 2.5°, when compared to our definition. We then use a formalism similar to that described by Ramsay et al. (2008) to convert discrete cyclone data into smooth gridded dataset. To generate this, we affiliate to each cyclone point an anisotropic Gaussian function, with an associated standard deviation of 1° and 3° in meridional and zonal directions respectively (Jourdain et al. 2010) and regrid it on a regular 2.5° × 2.5° grid. All other data are similarly gridded when necessary. In the following, the gridded dataset is used when spatial patterns are examined and the original data is made use of when time series or cyclone counting are involved.

Four sets of reanalyses are used to calculate the indices. NCEP-NCAR reanalyses starting in 1948 (NCEP: http://nomad1.ncep.noaa.gov/dods/reanalyses/reanalysis-1) and an "improved" NCEP–DOE AMIP-II reanalysis dataset (NCEP2: http://nomad1.ncep.noaa.gov/dods/reanalyses/reanalysis-2) starting in 1979. ERA-40 reanalyses are provided by ECMWF and the Japan Meteorological Agency. The Central Research Institute of Electric Power Industry (JRA25) reanalysis is also utilised. It is not the primary purpose of this paper to discuss the differences in these datasets and the reader is referred to Grotjahn (2008) for a thorough comparison between NCEP2 and ERA40. Our datasets are averaged into monthly means for the index comparisons. For coherence, all fields used in the index calculations are interpolated onto the NCEP 2.5° × 2.5° grid. Fields from January 1979 to December 2001 are used when comparing the differential influence of each reanalysis (as ERA40 finishes in August 2002 and NCEP2 starts in 1979).

Equations for the indices are described in the "Appendix" and are reproductions of otherwise published indices, namely the YGP index by Gray (1975), the CYGP by Royer et al. (1998), the GPI by Emanuel and Nolan (2004) and the TCS by Tippett et al. (2011). If they are to be used as assessive or predictive tools it is important that indices yield reasonable quantitative numbers. As mentioned in

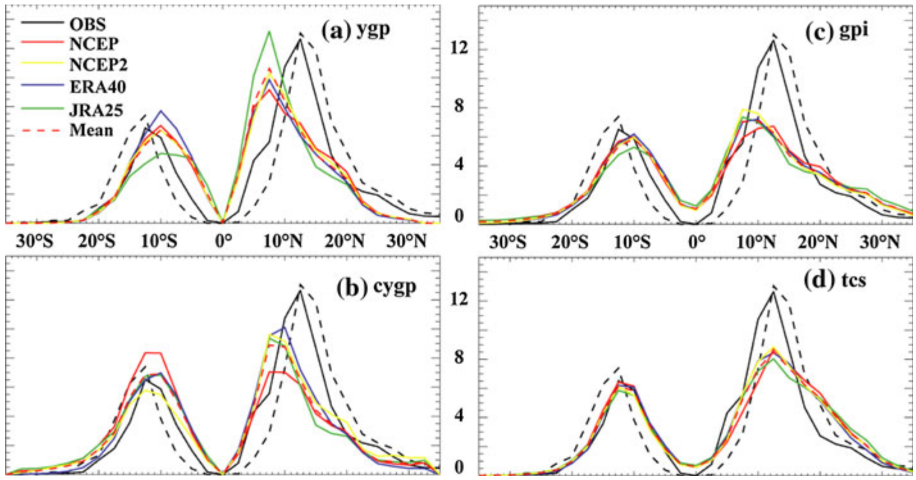

Fig. 1 Meridional distribution of zonally and time averaged observed and modelled cyclogenesis. In *black*, observed cyclogenesis defined by the first point in the dataset of storms that will reach 17 m/s along their track. In *dashed lines* observed cyclogenesis defined as the first position when storms reach 17 m/s. In *colours* mean cyclogenesis index distribution for the YGP (*top panel*), the CYGP (*second panel*), the GPI (*third panel*) and the TCS (*last panel*) using the four atmospheric reanalyses, NCEP (*red curve*), NCEP2 (*yellow curve*), ERA40 (*blue curve*) and JRA25 (*green curve*). The REM index (*see text*) is added on each panel as a *dashed red curve*

several studies, the "proportionality" constants (e.g. the 50 and 70 in the GPI, or the k in the CYGP, see "Appendix") are somewhat arbitrary and result from fit to the global and seasonal observed cyclogenesis data (Camargo et al. 2007a; McDonald et al. 2005; Caron and Jones 2008; Royer et al. 1998; Chauvin et al. 2006). Because these indices are all a priori dependent on the data sets used for their construction and the periods on which they are fitted to observations, the constants must necessarily be adjusted to match observed values. In order to compare all the indices on a common basis, it was decided to scale the indices calculated for each reanalysis by calculating the yearly number of tropical cyclones in the 30°S–30°N region for the 1979–2001 period amounting to ~85 cyclones/year in the range of previously published studies (Gray 1975, 1979; Tsutsui and Kasahara 1996; Royer et al. 1998; Royer and Chauvin 2009; Caron and Jones 2008; Kim et al. 2010). Kim et al. (2010) have also used a similar scaling in their analyses in order to compare all reanalyses and model outputs on common grounds. Discussion about such scaling can be found alongside the study and in the conclusion.

3 Results

3.1 Mean distributions

Figures 1, 2 and 3 present results for the mean distribution of modelled cyclogenesis. The indices have some skills in reproducing the first order meridional distribution of observations (Fig. 1). These distributions are consistent with previous studies (e.g. Watterson et al. 1995; Caron and Jones 2008; Royer et al. 1998, Tippett et al. 2011). Aside from the TCS, the other indices show too broad a distribution with simulated maxima that are too close to the equator by at least 2.5° independently of the reanalysis considered, especially in the northern hemisphere. By contrast, the TCS simulates the right maxima locations and the strong equatorial genesis decrease. Compared to the GPI, the accurate TCS behaviour is related to the use of "clipped" vorticity (see "Appendix") as discussed in Tippett et al. (2011).

The GPI shows particularly weak maxima in the northern hemisphere (Fig. 1) compared to the other indices but its interhemispheric balance (number of [30°S–0] cyclones over number of [0–30°N] cyclones) is the best among the indices (see Fig. 3). The GPI "weak" maxima (compared to the others) are partly due to the normalisation chosen. In fact, Figs. 1 and 2 show that the GPI has a tendency to overestimate cyclogenesis in regions outside the main cyclogenesis areas (e.g. off 20°N and within 10°S–10°N) (Camargo et al. 2007a). Therefore, normalising the GPI by a constant to ensure that the global count within (30°S–30°N) is 85 necessarily gives lower maxima amplitude in the main cyclogenesis regions compared to normalisation in a smaller latitudinal band. If another normalisation was chosen so that the number of modelled and observed cyclones agrees to within 20°S/20°N, the result would be that both the northern and southern maxima would be higher. Regardless, the southern maxima of GPI would not be well represented. In principle, the global indices could be adjusted to produce the right numbers in a given region but with the result that other regions would not agree with observations, as discussed further in the text.

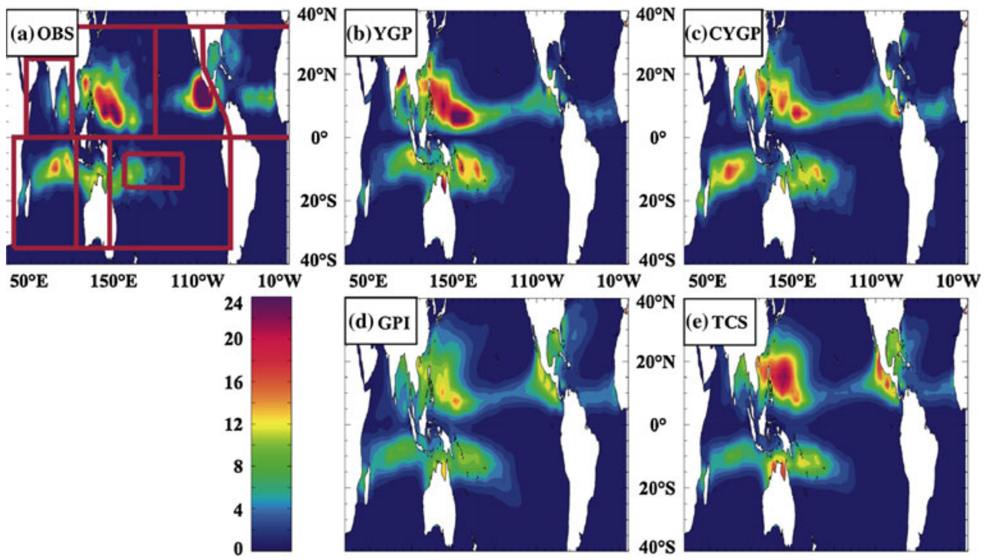

Fig. 2 1979–2001 mean cyclogenesis numbers per 5° and per 20 years for the observations (*panel a*) and all REM indices (*panel b* YGP, *panel c* CYGP, *panel d* GPI and *panel e* TCS). *Red boxes* noted on panel mark the regions used in the remainder of the paper and are defined in Table 1

Dispersion due to the choice of reanalysis is higher in the CYGP and the YGP than in the GPI and TCS where the reanalysis choice makes little difference. Except for the NCEP2-YGP, and NCEP-CYGP, all reanalyses produce coherent modelled cyclogenesis distributions. For the YGP, the use of NCEP2 leads to an underestimation of cyclogenesis in the southern hemisphere and overestimation in the northern hemisphere, when compared to other reanalyses. Such is not the case for the CYGP, thus pointing to the thermal term in NCEP2-YGP being responsible for its difference with NCEP2-CYGP (since the dynamical terms are identical). It appears that it is the strong north–south asymmetry of the shear temperature term (see "Appendix") calculated with NCEP2 that produces the north/south asymmetry compared with ERA40 or NCEP. A similar argument holds for the peculiar behaviour of NCEP-CYGP where, for instance, the ratio of north/south convective precipitation is weaker in NCEP than in NCEP2. Apart from these examples, there is better coherence for one index calculated using different reanalyses than between different indices sharing the same reanalysis. Hence, in the following, a "mean" index calculated as the average of that index with the four reanalyses, referred to as the "REM" index is often presented for clarity purposes (see dashed red line in Fig. 1), and the impact of specific reanalysis is only emphasized when needed.

Figure 2 provides the mean spatial distribution of cyclogenesis in observations and for the different REM indices. Figure 3 provides comparisons in the box-averaged regions drawn in Fig. 2 where the impact of the use of specific reanalysis is detailed. Large differences appear in the mean simulated cyclogenesis when compared to observations. For example, none of the indices are able to properly capture the cyclogenesis areas of the northeastern Pacific (see bottom panels on Fig. 3 and also Caron and Jones 2008 for a discussion on the YGP and CYGP using ERA40) even though the GPI and TCS show better spatial structures than the YGP and CYGP (Fig. 2). The YGP and CYGP simulate weak cyclogenesis in the western Atlantic compared to observations and to the GPI and TCS. On the other hand, the GPI overestimates cyclogenesis within 10°S–10°N and off 25°N. All indices also produce an unrealistic continuous cyclogenesis band along the ITCZ (Inter Tropical Convergence Zone) in the central Pacific. The genesis locations in the Bay of Bengal are also poorly reproduced in all indices (e.g. Caron and Jones 2008; Tippett et al. 2011). However, the TCS is in general the best-fitted index for such mean pictures.

This finding is also confirmed quantitatively in Fig. 3 when considering global northern and southern hemispheric averages (note that the boxes chosen and described in Table 1 are close to those of Caron and Jones 2008; also note that our results are very close to their Table 2 when calculated over the same time period and when taking into account the normalisation differences between the two studies). The relative error of the TCS on mean hemispheric numbers is less than 10% while the CYGP is shown to be the worst index based on that metric with a 50% overestimation in the southern hemisphere (Royer et al. 1998; McDonald et al. 2005; Caron and Jones 2008), mostly due to an overestimation of the southern Indian Ocean cyclogenesis; the GPI and YGP yield similar medium-quality results. Yet, these hemispheric figures hide large regional discrepancies that may compensate each other in the total hemispheric count. For example, the positive bias in the northwestern Pacific for TCS nearly

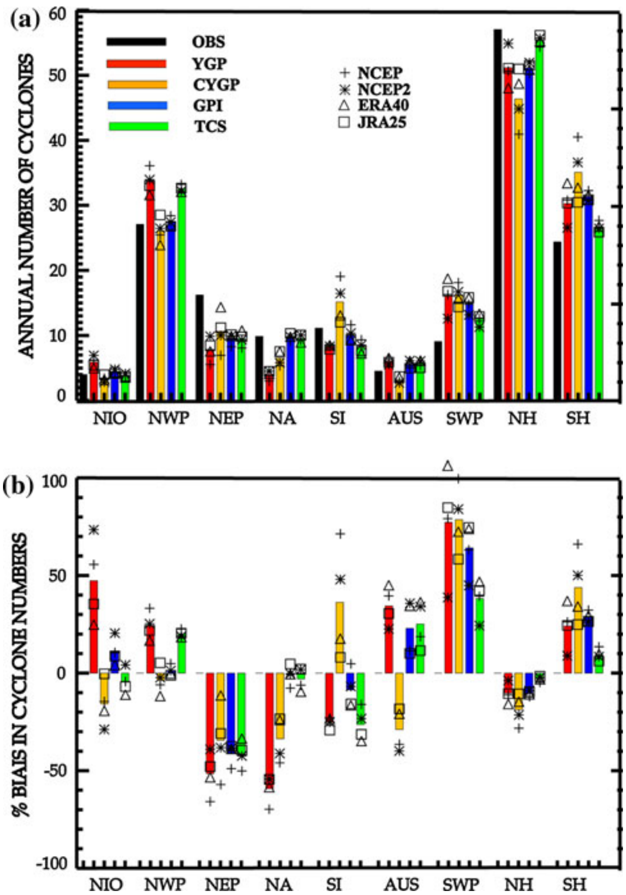

Fig. 3 Histograms of **a** annual mean number of cyclones in regions defined in Table 1 and shown in Fig. 2. In addition to the 7 boxes, total numbers for the northern hemisphere (NH) and southern hemisphere (SH) are shown for all indexes. These are labelled as *Y* YGP, *C* CYGP, *G* GPI, *T* TCS and *O* denotes the observations. The *colourbars* represent the numbers for the REM indices and each reanalysis result is added on each *colourbar* as follows: + NCEP, *open triangle* ERA40, *star* NCEP2, *open square* JRA25. **b** same as **a** but for the normalized differences to observations: (index-observation)/observations in percentage

Table 1 Definition of the geographical limits used in Fig. 2

Acronym	Longitudes	Latitudes
NIO North Indian region	45°E–100°E	EQ-35°N
NWP North Western Pacific	100°E–160°W	EQ-35°N
NEP North Eastern Pacific	160°W–90°W	EQ-35°N
NA North Atlantic	Atlantic domain	EQ-35°N
SI South Indian region	30°E–105°E	35°S-EQ
AUS Australian region	105°E–145°E	35°S-EQ
SP South Pacific region	145°E–70°W	35°S-EQ
SWP South Western Pacific	170°E–120°W	16°S–5°S

cancels out the negative bias in the northeastern Pacific so that the overall best agreement shown in integrated numbers using TCS is less apparent when looking regionally.

Hence, this quantitative comparison highlights the poor ability of the indices to reproduce the observed cyclogenesis numbers regionally, especially in the South Pacific (resp. Northeast Pacific) where cyclogenesis is overestimated (resp. underestimated) by more than 50% in all indices. The North Atlantic is poorly represented by the YGP and the CYGP while the GPI and TCS have good skills in that area. When examining the results as a function of reanalyses, the picture becomes more complicated. No dataset clearly outperforms any other in terms of all indices and regions, although using JRA25 seems to result in a relatively better estimation of mean cyclogenesis overall.

It is of interest to compare the respective contribution of each term to the total index. Because the index is a product of the partial terms, the most convenient way to quantitatively compare the term contributions is to examine the index logarithm, thereby expressing it as a sum of components. This method is used by Tippett et al. (2011) for the seasonal decomposition. Here we use the same method for mean patterns. Figure 4 shows the contribution of mean logarithms of the dynamical term for the different REM indices in percentages (thermal contributions are the complement to 100% of the dynamical component). The contribution of this term produces spatial variation that has no similarity in the indices. In terms of processes, the GPI and YGP compare relatively well, although with higher influence of the dynamics in the YGP. In the YGP, cyclogenesis is mostly dominated by the dynamical component everywhere, while in the GPI the thermal and dynamical terms are more equilibrated (however, when returning to the index itself, the contribution differences are necessarily enhanced). The CYGP has more spatially uniform dynamical contribution than the other indices while the TCS displays the largest meridional gradients. In pursuing this analysis, we focus on a specific region where dynamical terms are contrasted. Figure 5 presents the comparison for the North Atlantic region where all log terms entering the index composition are evaluated in percentage.

Firstly, Fig. 5 shows that the choice of reanalysis is globally unimportant when examining the mechanisms at work in the index constructions with concern to mean estimations (this is also true for other regions). Secondly, the relative contribution of all terms varies from one REM index to another. For example, the total dynamical (and thus inversely for the total thermal) terms vary from 40% in the TCS to 65% in the CYGP and the vorticity term varies from 10% (TCS) to 40% in the YGP. Note that the ocean content (HE) dominates the thermal term in the YGP as recorded by Royer et al. (1998). Obviously, the TCS and GPI have better skills at reproducing the observed numbers in the Atlantic (Fig. 3) and the YGP is by far the worst. With regards to the term partition, it is difficult to find an

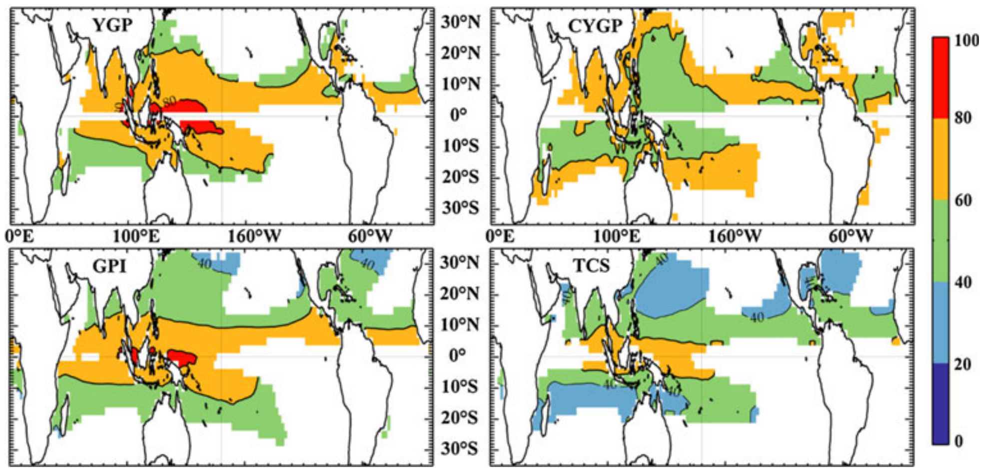

Fig. 4 Percentage of contribution of the dynamical term in the mean of each log index (see text for additional information)

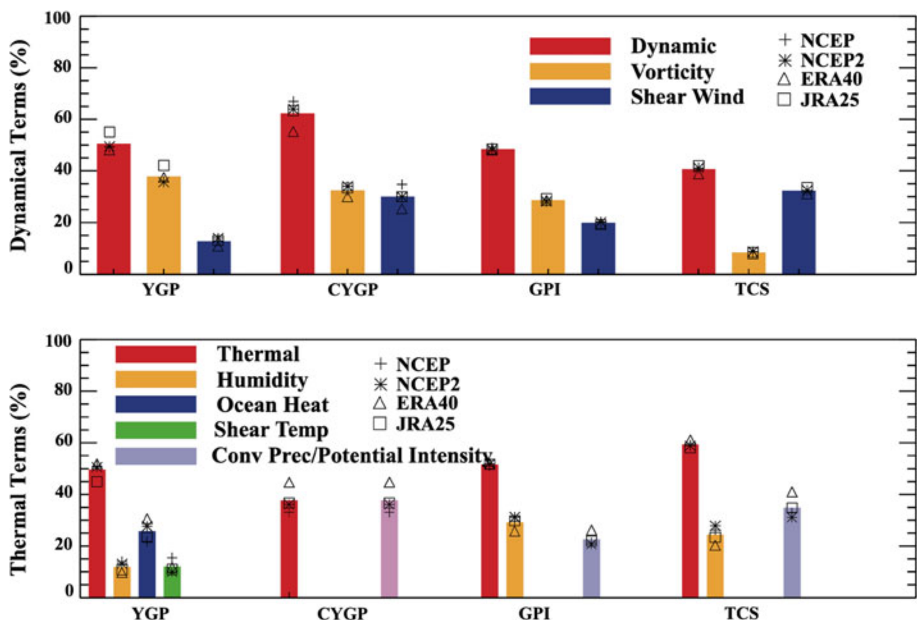

Fig. 5 Same as Fig. 4 but for all terms entering the REM index construction in the North Atlantic box (NA). *Y* YGP, *C* CYGP, *G* GPI and *T* TCS. For the individual term definitions, see "Appendix". The *first panel* represents the contribution of the dynamical terms: dynamical term (*red*), vorticity term (*orange*), wind shear term (*blue*). The *second panel* represents the thermal contribution. Thermal term (*red*), humidity term (*orange*), ocean heat term in the YGP (*blue*); temperature shear contribution in the YGP (*green*), convective precipitation term in the CYGP (*gray*). Potential intensity term in the GPI (*gray*) and SST term contribution in the TCS (*gray*). *Colour bars* are results for the REM indices and *symbols* on each *bar* present the results for individual reanalysis. These *symbols* are the same as those of Fig. 3

obvious bias that would point to any discrepancies or malfunction in the YPG. Interaction between the terms are complex and it may be that vorticity is too dominant in the YGP compared to GPI or that the wind shear and relative humidity terms do not have enough weight in the YGP, but going beyond these basic considerations would be difficult.

From these mean comparisons, it can be concluded that the indices are somewhat successful in globally reproducing the observed mean cyclogenesis at zeroth order independently of the reanalysis used. However, some unrealistic features also prevail. One instance of this can be seen in the northern hemisphere where an equatorward offset of modelled cyclogenesis by 2.5°–5° can be seen in all the indices except the TCS. They can reproduce cyclogenesis numbers in some specific regions using a constant global scaling (Kim et al. 2010) but not everywhere. The indices can always be adjusted to give the best reproduction of a specific mean number regionally but this is at the expense of degrading another region because the biases are not homogeneous. Alternatively, an *ad hoc* correction can be designed to adjust mean simulated data to mean observations everywhere but this does not actually enhance index performances on other timescales (see "Discussion"). Finally, it is difficult to estimate the actual quantitative contribution of a given mechanism in the indices because the relative contributions can vary significantly from one index to another.

Overall, the TCS seems better adjusted to simulate the mean cyclogenesis but detailed regional comparisons show that regional biases may still be important and that they depend on the chosen reanalysis.

3.2 Seasonal variations

In this section we assume that the indices are best fitted to the observed climatology. Box averaged times series are shown in Fig. 6. The boxes chosen are also close to those presented on Fig. 4 of Camargo et al. (2007a) and on Fig. 7 of Tippett et al. (2011). As earlier, the indices agree and disagree with observations in various ways. All indices have a correct seasonal cycle except for the YGP and, to a lesser extent, the CYGP in the north Indian region (see following discussions on the individual terms). The results presented here are coherent with other studies. The TCS is the best fitted for the global seasonal cycle especially in the northern hemisphere, although not everywhere (e.g., the northwestern Pacific during the peak season). This is another illustration of the need for individual regional examinations to properly evaluate any index. The TCS is also the only index that minimises the discrepancy with observations during the unfavourable season. Variations between indices are huge in the North Atlantic where the CYGP and YGP seasonal variations are too weak. Bruyere et al. (2010) also emphasized that the GPI showed biases in the Gulf of Mexico regions to the extent that little confidence could be given to the spatial structure of that index. Note also that the dispersion between indices is relatively important at peak seasons, except for the South Pacific box. Again, the northeastern Pacific region is systematically underestimated. Such a seasonal picture given by the REM indices, is quite similar to that using individual reanalyses (not shown). The dispersion of one index using different reanalyses is far weaker than that of the indices using the same reanalysis.

Attention is now turned to the mean contributions where all indices are now examined to discover how the different terms contribute to the seasonal cycle of the index logarithm. A similar analysis can be found for the TCS in Tippett et al. (2011). Although this is only an analysis of the log contribution, their variations reflect those of the actual terms since exponential is a monotonically increasing function. The method consists of calculating the seasonal anomalies of the individual term logarithms so that the seasonal anomaly of the total index logarithm is the sum of all individual seasonal logarithmic anomaly terms. Figure 7 presents the cases of the northern hemisphere and the North Indian Ocean where TCS and GPI are the best-adjusted indices and the YGP does not perform well. In order to compare the relative influence of terms between indices, all curves for a given index are normalised by the maximum value of the seasonal index logarithm in each box so that all terms vary within ±1. Behaviour in the

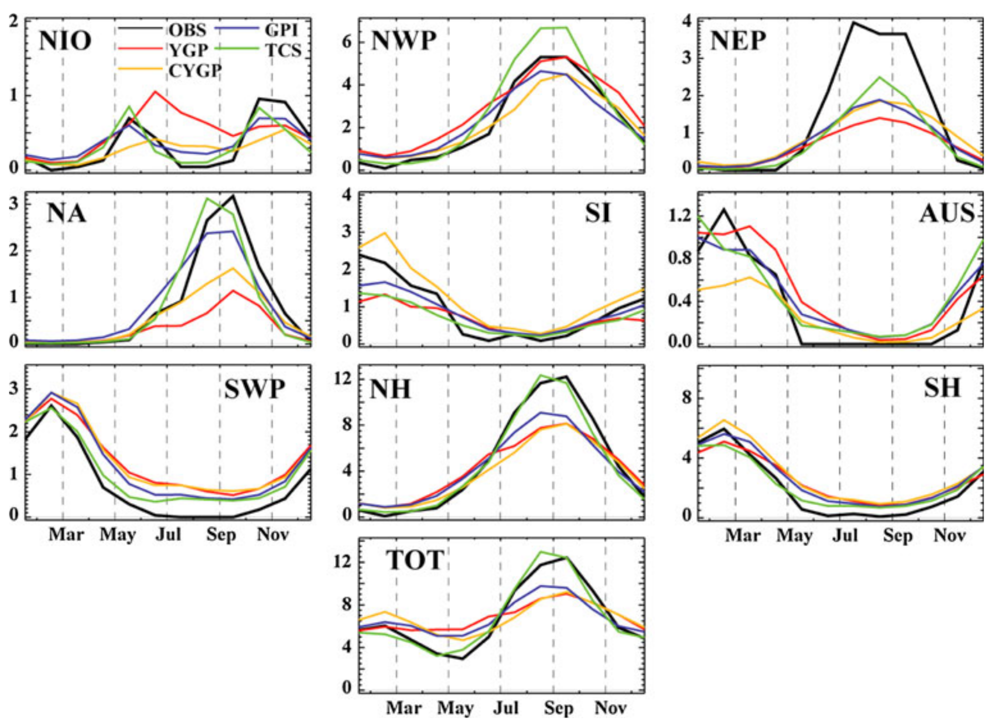

Fig. 6 Seasonal variations of observed cyclogenesis (*black*) and REM indices in all *boxes* of Fig. 2. This goes for the northern and southern hemispheres as well as for the globe which are all labelled in the titles. Observations are in *black*, YGP is in *red*, CYGP in *orange*, GPI in *blue* and TCS is in *green*

northern hemisphere is representative of all other regions (not shown) except the north Indian Ocean region. The (logarithmic) YGP seasonal cycle is always dominated at 80% by seasonal variation of the thermal potential, itself dominated by the ocean heat content (Royer et al. 1998). The remaining 20% can be explained by variations in wind shear and surface vorticity. By contrast, the CYGP is strongly dominated by the dynamical term (see previous section) with an almost equal interplay between vorticity and vertical wind shear terms. In retrospect this is surprising as the CYGP thermal potential was designed to simplify the YGP thermal potential. The GPI offers a more delicate balance where the thermal potential dominates the seasonal variations ($\sim$60%) but where all terms (except vorticity) play an equivalent role. Note that the thermal potential variations are in fact due to the interplay of the PI and relative humidity terms. In the TCS, the partition between dynamical and thermal is almost identical with the thermal term being slightly dominant. Again vorticity plays a minor role in explaining the seasonal variations but when compared to the GPI, relative humidity plays a weaker role in the thermal term, which instead is dominated by variations of the SST index (Tippett et al. 2011).

The north Indian Ocean cyclogenesis (enhanced in the Bay of Bengal) is unique in that it shows two peaks. The phasing of these peaks is best reproduced by the GPI and TCS (Fig. 6). The YGP picture is more complex with all terms coming into play at one moment or another. During the first season, the index peaks with a 1-month delay (Fig. 6) when compared to the other indices and observations. This can also be seen in the log index. The 1 month delay is explained by the existence of a delay in the thermal component related to humidity. This humidity effect dominates the thermal component in June-July. The delay is further explained by noting that the dynamical term decreases during the observed period and does not compensate for the thermal component increase. By contrast, in the other indices the dynamical component dominates the index decrease. It seems clear that the overall parameterisation of the YGP is at fault, but as the interplay between the terms is quite intricate and interdependent, which specific term is to blame (if any) could be difficult to explain. It is of interest to also note that in the CYGP, the dynamical terms can vary in opposition, contrary to the TCS and GPI, and even to the YGP (compare the vorticity terms—blue dash in all panels). The TCS and GPI exhibit similar behaviours but the respective term balances vary significantly between the two indices, although both reproduce the observed peaks with some success. Tippett et al. (2011) also analyse cyclogenesis variations in this region via the individual TCS terms. Our analysis with the CYGP and GPI support their findings: that pre-monsoon reduction in wind vertical shear creates the pre-monsoon maximum and that its increase leads to the decrease of the first genesis peak. Our analysis also suggests that the mechanisms at work quantitatively differ according to the index.

Overall, even if the indices have been historically adjusted to simulate seasonal cyclogenesis, it can be seen that for the annual mean and seasonal cycle, caution is still needed in reference to their ability in explaining observed regional cyclogenesis. Index performances differ globally and regionally and one conclusion drawn using a single index may not hold for the others. This is also true when seeking cyclogenesis mechanisms from these indices. At best, they can only give qualitative indications regionally and we advise caution in drawing firm conclusions. The complex interplay between individual terms prevents an easy understanding of the parameterization flaws that lead to misrepresentation of cyclogenesis. Eventually, it might be possible to pin point index defaults in one basin by readjusting the index parameterisation in a given region and comparing that new parameterisation to the global one, thus allowing a characterisation of the distance between the global and the regional parameterisation. However, this is beyond the scope of the present paper.

3.3 Interannual variations

There have been relatively few studies that explore the pertinence of cyclogenesis indices on interannual timescales in the present climate. Watterson et al. (1995) used the YGP to describe and understand how is cyclogenesis influenced by large scale forcing, using ECMWF analysed fields (1979–1988). After exploring the YGP's ability to reproduce observed interannual variability with particular emphasis on ENSO they concluded that the index has limited success in terms of observed variability reproduction. They particularly noted that the amplitude of simulated cyclogenesis is much weaker than that observed. Camargo et al. (2007a) detailed the GPI patterns associated with ENSO and concluded that the index "successfully reproduces the most well known ENSO signals in the best-observed basin". Camargo et al. (2007b) went into further details by looking at sub-basin interannual variability and emphasized the need to investigate ENSO impact on regional rather than basin-wide scales. To evaluate the interannual skill of the GPI, the focal point of the research focussed on correlation patterns with limited quantitative estimates of interannual cyclogenesis numbers. Lyon and Camargo (2009) used the GPI to understand ENSO impact on TC genesis in the Philippine region, which was shown to qualitatively agree with patterns of observed cyclogenesis. Vincent et al. (2009) used the CYGP to understand the differential impact of ENSO phases on TCs in the South Pacific Convergence Zone (SPCZ) region. These studies

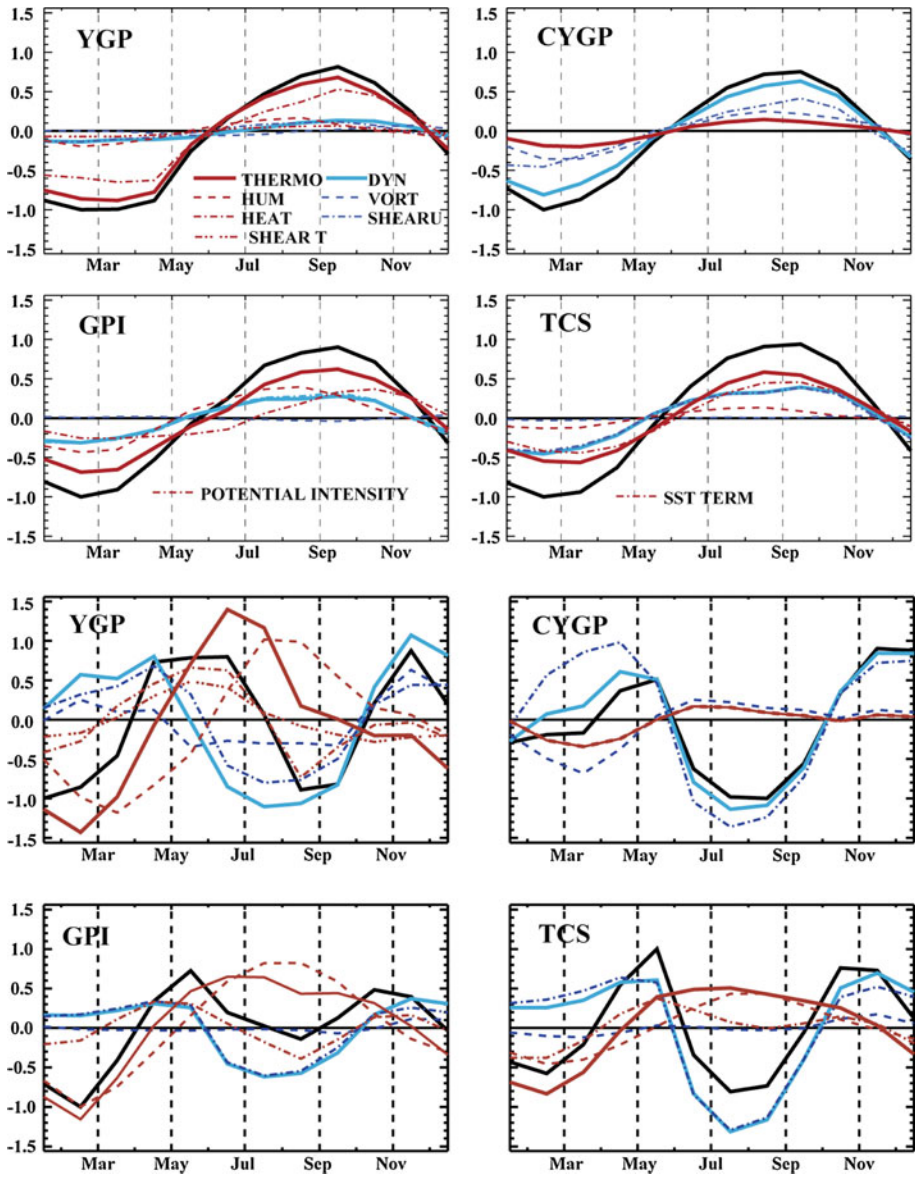

Fig. 7 Contribution of all terms in the seasonal variations of log index for each REM index. The northern hemisphere box is illustrated in the *first four panels* and the north Indian Ocean is shown in the *last 4 panels*. In *black* the total variations of the log index is represented. In *blue* dynamical terms with the total dynamical term being represented as a plain *blue curve*. In *red* thermal terms: total thermal term in plain *red curve*. *Dashed red* is the humidity term, *dashed-dotted red* is the ocean heat contribution for the YGP, *dashed-doubled dotted red* is the temperature shear term. For the GPI, *dashed-dotted red* is the potential intensity contribution and for the TCS, *dashed dotted red* is the SST index contribution. For the dynamical terms (*plain blue*), *dashed blue* is the vorticity term and *dashed-dotted blue* is the wind shear term contribution

also agreed on the usefulness of the indices in understanding certain underlying physics of cyclogenesis on interannual timescales. Finally, Tippett et al. (2011) also examined interannual variability and showed that results using the ERA40 reanalysis were significantly different from those using NCEP and that ERA40-TCS showed considerably more variability than NCEP-TCS. They also concluded that the correlation levels of TCS versus observations were "roughly" similar to those found in Camargo et al. (2007a).

In this paper, we build upon these studies by exploring, at the global scale, the skills of all indices and reanalyses in reproducing interannual variability. Figure 8 presents the interannual standard deviation of all REM indices and observations. The most striking feature of this figure is that it shows systematic failure of all indices to reproduce observed interannual amplitudes. Such low variability indicates that there is little chance that these indices can be used to simulate accurate interannual variations in worldwide TC numbers.

For a more precise illustration, box-averaged time series are presented in Fig. 9 with corresponding statistics in Fig. 10. These figures show that all the indices tend to agree on their regional discrepancies with observed variability. The failure to reproduce the north Indian Ocean interannual cyclogenesis is coherent with previous studies (e.g. Tippett et al. 2011). None of the indices are able to produce significant correlation with observations in the South Indian region, except for the CYGP using NCEP and ERA40. The NCEP2-CYGP and JRA25-CYGP were examined to understand why they did not produce acceptable cyclogenesis compared to NCEP-CYGP and

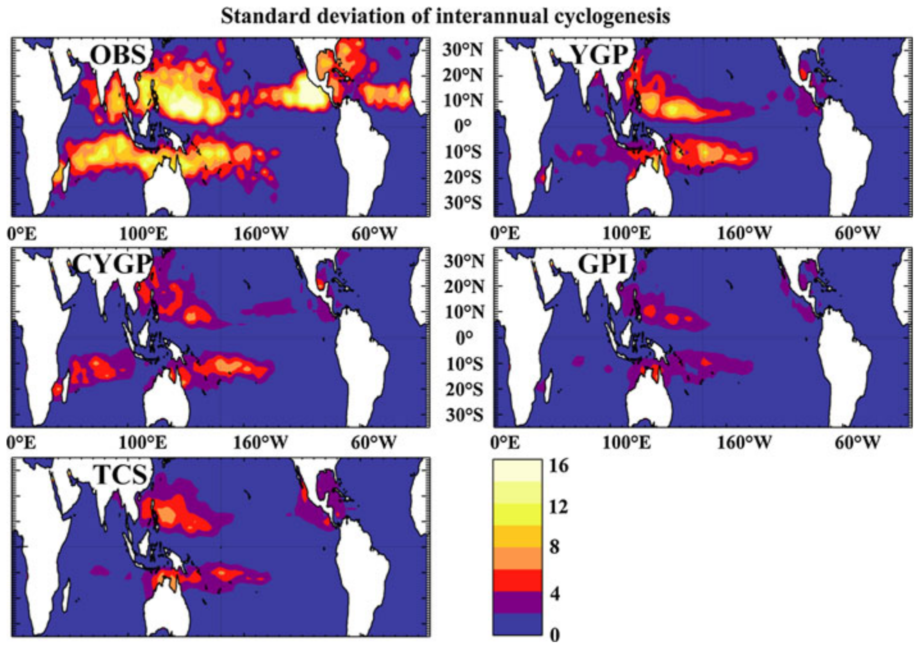

Fig. 8 Standard deviation of interannual cyclogenesis from observations (*top*, *left panel*), and REM indices. Units are numbers per 5° and per 20 years

ERA40-CYGP but a clear conclusion could not be reached. Moreover, with the exception of the CYGP, the north-western Pacific variability is not reproduced by the indices. It seems clear that the success of the CYGP there is linked to its parameterisation of the thermal potential. That stated, it is still unclear what changes need to be made in the other indices to reach the correct variability. When looking at the time series (Fig. 9, panel B), the CYGP is not obviously better than the other indices and a few peaks in phase with the observations probably make the correlation significant for the CYGP, in contrast to the other indices.

Phase relationships in other regions are globally reproduced by all indices but with varying performances. The usual correlation of indices to observations is about 0.5 and does not exceed 0.7. It also varies from one index to another and depends on the region under consideration. With a few exceptions, the choice of reanalysis has relatively little effect on performances. Also note that ERA40 is the only reanalysis that produces significant correlation with the YGP, CYGP and GPI in the northwestern Pacific. Again, the reasons for this are not obvious. Figure 9 also shows that on interannual timescales, the GPI and the TCS usually exhibit similar performances except in the north-west Pacific where all indices differ, with bad performances as depicted above. Strikingly enough, in Figs. 9 and 10 the bottom panel shows that for region-wide averages the interannual indices generally do poorly at representing the amplitude of interannual cyclogenesis and that there are wide variations within regions, indices and reanalyses. It must be noted that these results are (only) a more detailed confirmation of those inferred from Fig. 8. The only region where interannual standard deviation may be in relative agreement with observations for all indices is the north-western Pacific but, again, phase variability is poor when compared to observations (Fig. 9).

As in the previous section, the influence of each term entering the indices is evaluated. Unlike the previous section, here it is possible to isolate each term's influence in the total interannual index using a Taylor expansion of the total indices with respect to their seasonal cycle. A similar method applied to climate change evaluation is used in Kim et al. (2010) (see their Eq. 2). Hypothesizing that the interannual deviations are small compared to the seasonal cycle, the index interannual signal can be written as:

$$I_{\mathrm{total}}^{\mathrm{INTER}} \approx I_{\mathrm{total}}^{\mathrm{SAIS}} \left(\sum_{z=\mathrm{terms}} \left(I_z^{\mathrm{INTER}} - I_z^{\mathrm{SAIS}} \right) \Big/ I_z^{\mathrm{SAIS}} \right)$$

It was verified that such approximation is valid with less than 5% error except off 20°N in the CYGP and YGP indices. The advantage of this method is that it allows estimating the real contribution of any term in the total index at interannual timescales. Once each term contribution has been calculated for all indices, these terms are then regressed to the total interannual signal at each grid point. Results in Fig. 11 are only displayed when the significance of the correlation between the interannual index and each term exceeds 90%. Some of the terms have been omitted in this figure for clarity, but, for instance, the contribution of the wind shear to the total signal can be deduced from the difference between the dynamical and the vorticity contributions. Similarly, the thermal contribution to the total index is the complement to 1 of the dynamical contribution. Figure 11 shows that the

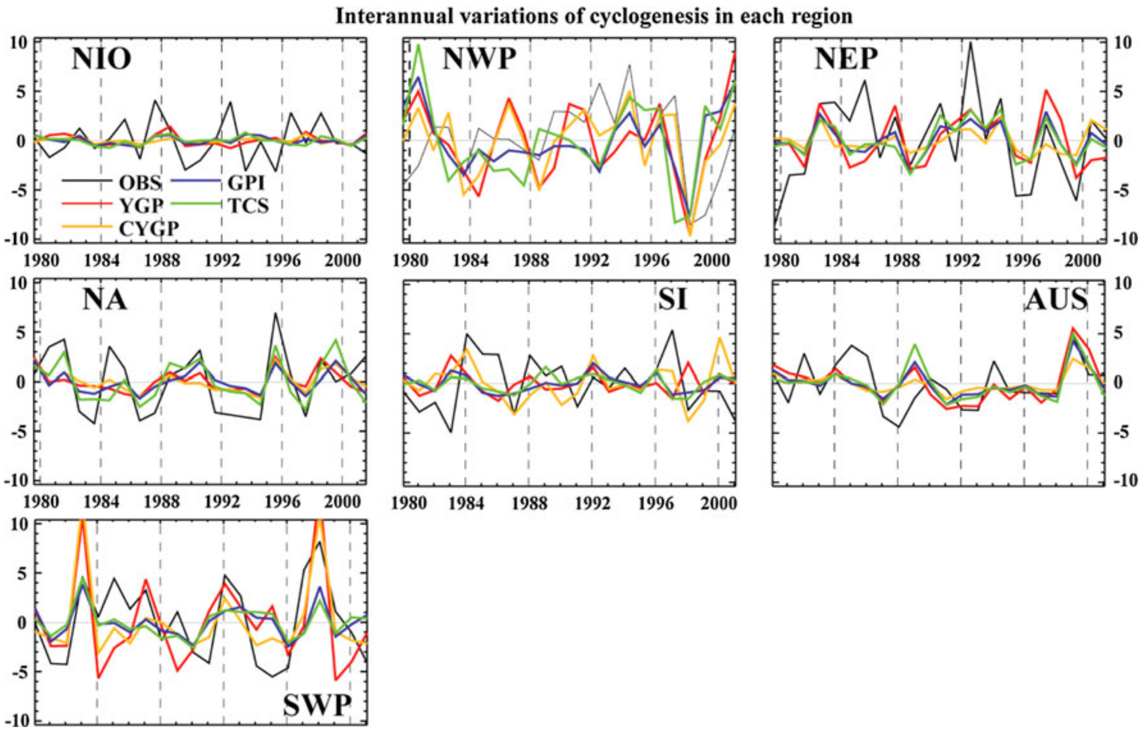

Fig. 9 Time series of yearly observed and REM interannual cyclogenesis anomalies in boxes depicted in Fig. 2. Observations are in *black*, YGP in *red*, CYGP in *orange* and GPI in *blue* and TCS is *green*

dynamical contribution to the total index strongly depends on the index and the region considered. On the global scale, this contribution is larger in the CYGP than in the other indices. Overall, the CYGP and YGP term partitions are closer than for the TCS and GPI. North of 20°N, our separation method shows large errors for the CYGP and YGP which cannot be significantly separated into terms. In this region, interannual cyclogenesis from TCS and GPI are dominated by thermal terms. Because the previous figures have shown the inability of these indices to reproduce observed interannual variability in the northwest Pacific, we maintain that the partition shown in the TCS and GPI may not be appropriate. The partition between vorticity and shear also differs among indices (and regionally).

Strikingly, the interannual variability of cyclogenesis in the SPCZ region (denoted by the black line, see legend) is strongly dominated by vorticity in the YGP and CYGP (Vincent et al. 2009) but far less so in the TCS and GPI. At the same time all indices yield similar performances in terms of phase variability (Figs. 9, 10). The CYGP and YGP are however in better agreement with observations in terms of amplitude (Figs. 9, 10). In light of the term partitions, it may thus be that a stronger dynamical influence on the final index is required in the TCS and GPI formulation to yield the most realistic amplitude. South of the SPCZ and around Australia, interannual cyclogenesis is dominated by the thermal influence but the partition between the thermal terms varies significantly among indices. In the North Atlantic, where TCS yields the best interannual cyclogenesis, the partition between SST and relative humidity effects is almost equal in contrast to the GPI where humidity dominates.

The major flaw of all the indices at interannual timescales is their weak simulated amplitude of interannual variability. Evidently, the index amplitudes are directly connected to the normalisation chosen. In this study we used a global normalization, but a regional amplitude correction may yield improvements on interannual variability (see Kim et al. 2010 for a discussion as well as our concluding remarks). Finally, it appears from analysing the genesis index components that there are significant differences between the working mechanisms of each index. Index partitioning may be used on occasions for future index diagnostic improvements, but, to a limited extent, as the simulated effect of an environmental variable (i.e., humidity or vorticity…) is subject to the somewhat arbitrary choice of its functional form. Nevertheless, one outcome of such analysis is that the respective effect of each term appears to vary at a lower scale than that used for box-average quantification. For instance, cyclogenesis mechanisms around Australia differ from those involved in the SPCZ region. Therefore, analysing cyclogenesis in a large inhomogeneous region may be inappropriate (e.g. Camargo et al. 2007b and the following discussion).

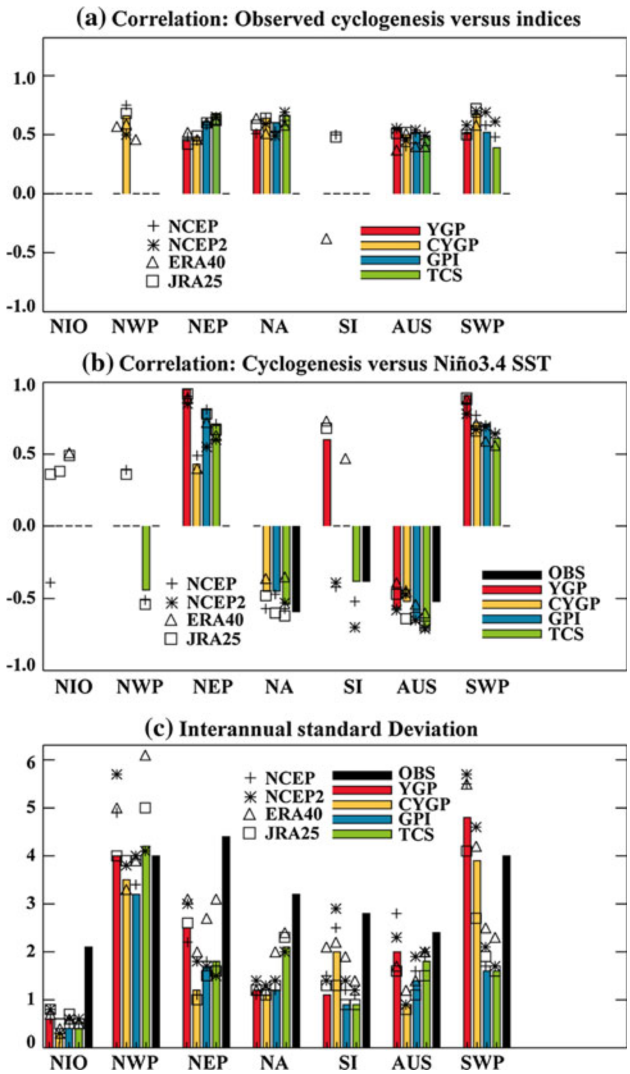

Fig. 10 Histograms of **a** correlation of box-averaged interannual observed cyclogenesis and REM indices. **b** correlation between box-averaged interannual cyclogenesis from REM indices and NINO3.4 (*red* for YGP-NINO3.4, *orange* for CYGP-NINO3.4, *blue* for GPI-NINO3.4 and *green* for TCS-NINO3.4) and between observed cyclogenesis and NINO3.4 (*black*). **c** Interannual standard deviation of box averaged time series of REM indices (*colours*) and of observed cyclogenesis (*black*). Other *symbols* and *labels* in the figure are identical to those of previous figures. Individual reanalysis results are labeled with + NCEP, *open triangle* ERA40, *star* NCEP2, *open square* JRA25; only >90% significant correlation are shown. NINO3.4 is calculated as the SST anomaly time series in the 120°W–170°W and 5°S–5°N region (e.g. Trenberth 1997)

3.4 Interannual variations: ENSO

As widely discussed (e.g. Chu 2004; Camargo et al. 2007a, b; Tippett et al. 2011 and references therein), ENSO is a major contributor to the interannual variability of cyclogenesis and induces regional cyclogenesis differences. Typically, ENSO induces large-scale cyclogenesis displacements that result in dipole patterns in observed cyclogenesis anomalies as well as in indices such as the GPI (e.g. Camargo et al. 2007a; Lyon and Camargo 2009). Such dipole patterns in the SPCZ region are detailed in Vincent et al. (2009), Jourdain et al. (2010) using observations, high-resolution model simulations and the CYGP. Figure 12 shows the correlation between ENSO, observed cyclogenesis, and index simulation. It should be used along with Fig. 13 that presents the actual Niño-Niña composites over the time period (see legend for the years over which the composite is calculated). The first panel of Fig. 12 shows that all regions of high-observed interannual variability exhibit a phase relationship to ENSO but with varying significance and correlation level. It is of interest that maximum correlation rarely exceeds 0.7 locally and the largest coherent patterns of correlations between ENSO and observed cyclogenesis are located in the southern hemisphere and in the central North Pacific.

The proximity of positive and negative correlations in Panel 1 of Fig. 12 primarily indicates spatial shifts in cyclogenesis activity from Niño to Niña phases, which can be seen in Panel 1 of Fig. 13. As an example, the northwestern Pacific region shows a significant dipole pattern that corresponds to a southeastward shift of cyclogenesis during El Niño years. With the exception of its southern edge, the northeastern Pacific shows a poor correlation with ENSO while its interannual variability is large (Figs. 8, 9, 10). In this example, ENSO does not seem to be a major driver of interannual cyclogenesis. However, other interannual processes seem to be at work (see Chu 2004 for additional discussion). Nevertheless, ENSO mainly has a tendency to decrease cyclones off the coast of Mexico (Fig. 13). Similarly, in the North Atlantic Ocean, ENSO influence on cyclogenesis is limited to the Gulf of Mexico, and the ITCZ, with a tendency for weaker cyclogenesis during El Niño and stronger during La Niña. The South Pacific shows the largest regions of significant correlation The Australian region is coherently and negatively correlated to El Niño in agreement with numerous other studies (see Ramsay et al. 2008, for a recent and exhaustive review of that region). From ~160°E to the eastern Pacific, a large pattern of positive correlation is visible and bordered to an extent by negative correlation in the south. Positive and negative patterns are established along a northwest/southeast axis (see Fig. 15) that corresponds to the maximum cyclonic relative vorticity associated with the SPCZ (Vincent et al. 2009). Cyclogenesis changes on ENSO timescales (as detailed in Vincent et al. 2009) have strong constraints imposed by the SPCZ dynamics and its north/south and east/west movements. In the South Indian Ocean, negative correlations with ENSO are consistently found in observations from western Australia to about 70°E and correspond to decreased cyclogenesis (Fig. 13). Because of the dipole patterns discussed above, box averaged

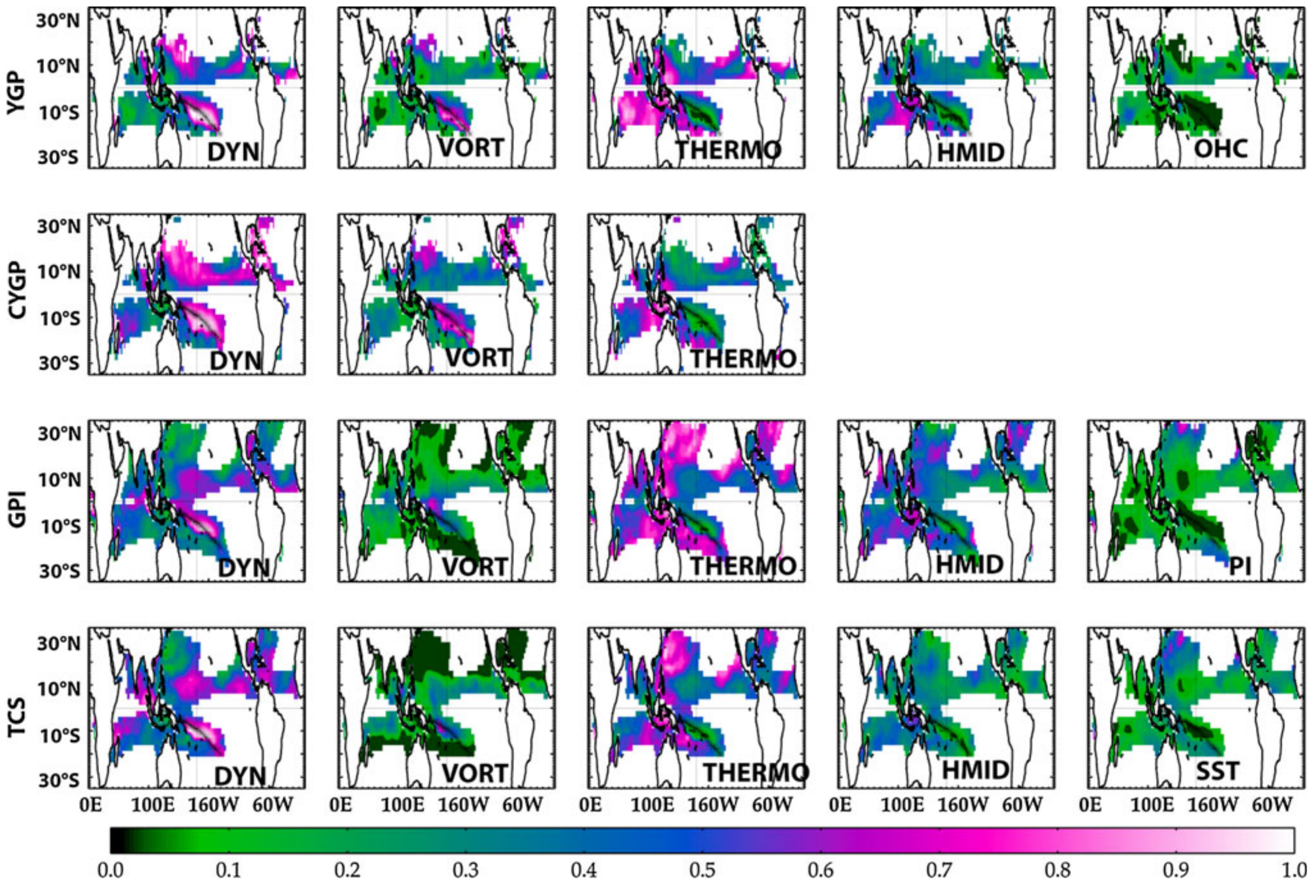

Fig. 11 Regressions between selected terms of the REM index and the REM index for each index. *First line panels* the YGP analysis, *second line* the CYGP, *third line* the GPI and *fourth line* the TCS. A *black line* on each panel in the southwest Pacific represents the mean SPCZ position as calculated by the maximum precipitation from CMAP (Vincent et al. 2009)

correlation of ENSO with TC genesis in large regions such as those presented in the boxes of Fig. 2 should be weak, as mentioned by Camargo et al. (2007b). Indeed, as seen in the middle panel of Fig. 10 (see black bars), it is striking that it is only in those regions where ENSO has a coherent impact on TC (see first panels of Figs. 12, 13) that box-averaged correlations are significant.

By contrast, box-averaged indices can exhibit significant correlations with ENSO whereas the observations do not (middle panel in Fig. 10) This can be seen in the South Pacific or in the northeastern Pacific. This seems to suggest that the indices can occasionally overestimate the cyclogenesis impact of ENSO. This is confirmed in Fig. 12 where ENSO dipole patterns are clearly depicted by all indices but with more coherent spatial structures and higher correlation numbers than in the observations (compare the top left panels with the others). Again in Fig. 12, we have limited the index-ENSO correlation to the regions where the observed interannual standard deviation is greater than 1 (see Fig. 8) but the pattern of index-ENSO correlation is much wider than in the observations. Therefore, it can be seen that on the one hand all the indices have obvious skills in characterising the typical TC genesis shifts under ENSO conditions, yet based on the present dataset, they also tend to overestimate the influence of ENSO onto TC genesis. This latter point is not very surprising as the indices represent *the potential* for cyclogenesis which cannot be reached in reality as stochastic effects may be important (Jourdain et al. 2010). This point is further discussed in the conclusion. Figure 13 provides another way of more precisely validating the ENSO effect on TCs. With reference to the correlation patterns of Figs. 12, 13 shows that the indices are globally successful in reproducing the observed Niňo-Nina patterns, even if quantitatively in certain areas the general tendency is to underestimate the numbers almost everywhere (as discussed before). Again, this general statement does not always hold true. For example, in the eastern Pacific, the Atlantic ITCZ, and in the south Indian Ocean, ENSO impacts on cyclogenesis are not reproduced by the indices. In the northwestern Pacific, the TCS shows the best skills (see the middle panel of Fig. 10) while the CYGP is strongly biased. Referring back to the South Pacific and with the exception of the YGP, the composites from all the indices are coherent with observations, albeit with weaker amplitude.

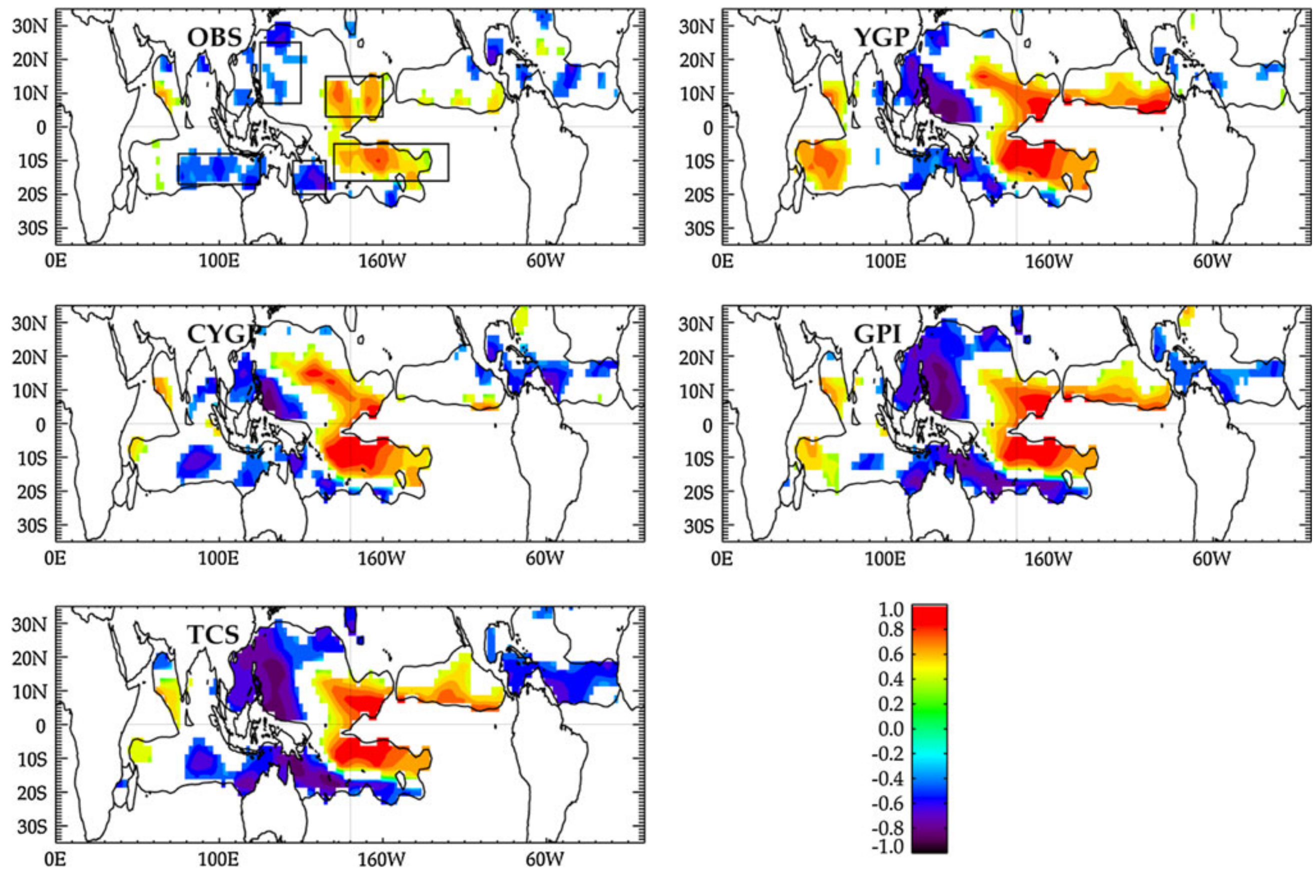

Fig. 12 Correlation maps between the interannual cyclogenesis anomaly and Niño 3.4 index. *Top left panel* correlation between observed cyclogenesis and Niño 3.4. Only >90% significant correlation is shown. Correlation patterns are limited to the region where interannual standard deviation numbers are greater than 1 (Fig. 8), as depicted by a *thin black* contour. *Other panels* same as the first except for all REM indices calculated. On the *top left panel black boxes* used in Fig. 14

Kim et al. (2009) have shown that not all El Niño types impact cyclogenesis identically in the North Atlantic (see their discussion on the differential impacts of eastern Pacific versus central Pacific warming). Similarly, Vincent et al. (2009) have shown that a strong asymmetrical El Niño mode exists with a distinct impact on cyclogenesis as discussed above. Hence, it may be that Figs. 12 and 13 would change when the influence of the El Niño types are considered separately. This is of great interest, yet the limited length of data used here does not allow a quantitative exploration and is left for future investigation.

It is of interest to evaluate the index performances at their best within the regions of coherent patterns rather than in large boxes averaging dipole patterns. Thus, Fig. 10 is reproduced, except in coherent correlation and pattern regions depicted in Figs. 12 and 13 (see black boxes). These results are presented in Fig. 14. As expected, choosing coherent sub regions yields higher and more significant correlation numbers both between indices and observed cyclogenesis (compare top panels, Figs. 10, 14) but also between indices and ENSO (second panels, Figs. 10, 14). Correlations to ENSO are usually higher than those with observed cyclogenesis, suggesting again that the indices have better skills at simulating the cyclogenesis impact of ENSO than at simulating the interannual TC variability in general. Figure 14 also confirms that the indices can overestimate the TC genesis impact of ENSO compared with observations (for example, see the northwestern Pacific box where the correlation between observed cyclogenesis and ENSO is lower than that computed with the indices). Yet, the bottom panel of Fig. 14 clearly shows that in most cases (with the exception of the SPCZ region for the CYGP and YGP and the northwestern Pacific for the YGP and TCS), the amplitude and the interannual indices are usually much lower than that observed (Fig. 8).

Finally, we have performed a similar analysis as presented in Fig. 11 for the terms dominating the interannual indices during ENSO. This is done by regressing all the interannual index terms to ENSO. Figure 15 shows that, unlike the diversity discussed in Fig. 11, all indices have good agreement on the dominant mechanisms modifying the index cyclogenesis during ENSO. Retrospectively, this gives additional support and credibility to the conclusions

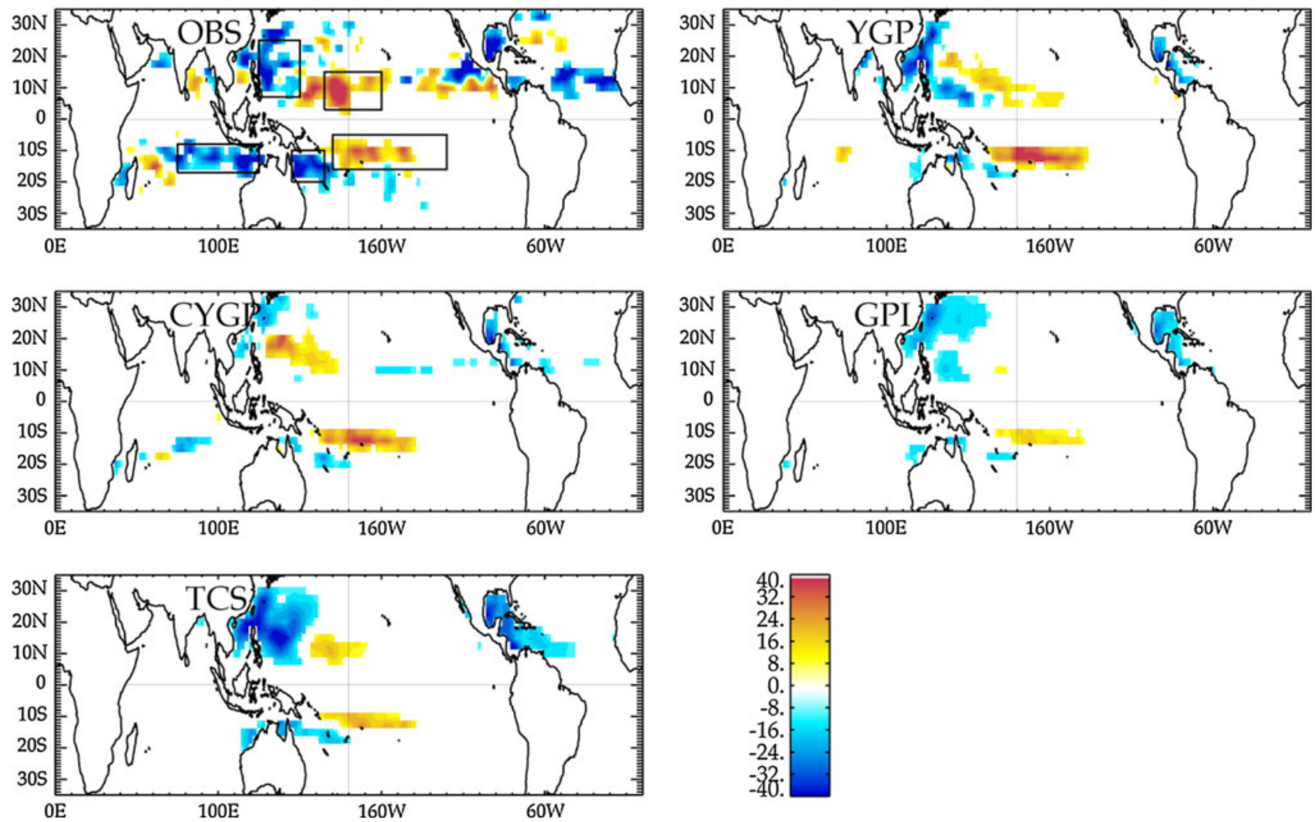

Fig. 13 Composites of cyclogenesis number differences between Niños and Niñas for the observations (*top left*) and the REM indices. Units are in cyclones/20 years/5°. The southern hemisphere shows the signal for the January–March composites while the northern hemisphere shows the signal for the August–October composites. Years entering Niño composite are for the southern hemisphere: 1983, 1987, 1992, 1995, 1998 and for the northern hemisphere: 1982, 1986, 1987, 1991, 1994, 1997. Years of Niñas composites, are for the southern hemisphere: 1985, 1986, 1996, 1999 and for the northern hemisphere: 1988, 1998, 1999

reached by Camargo et al. (2007a), Vincent et al. (2009) and other studies using one index and one reanalysis. To concentrate in regions where ENSO correlates significantly with observed cyclogenesis (black boxes in Fig. 12) and in regions where these regressions are significant, strong conclusions about the mechanisms at work can be drawn. An example of this is in the north central Pacific box where TC genesis increases during El Niño primarily in response to increased vorticity, followed by decreased wind shear, and to a lesser extent, by increased humidity. In the southern hemisphere and north of the mean SPCZ position, mechanisms are identical at first order although with an even stronger dominance of the vorticity increase. This is due to the peculiar asymmetric mode that occurs in the SPCZ on ENSO timescales (Vincent et al. 2009). To the south of the SPCZ and in the Australian region, cyclogenesis decrease during El Niño is mainly driven by thermal changes, such as decrease of mid-tropospheric relative humidity and other thermal terms (e.g. the SST index in the TCS, the PI index in the GPI etc…). To a lesser extent, it is driven by the wind shear term (increased wind shear; see Ramsay et al. 2008) but vorticity does not play a major role. This role of mid-tropospheric humidity agrees with the findings of Camargo et al. (2007a) but seems to disagree with the dominant mechanisms evoked in the analyses of Ramsay et al. (2008) who examined direct correlation between TCs and environmental variables such as vorticity and vertical wind shear during ENSO. In particular, they suggest that the causal relationship between vorticity and TC numbers over northern Australia is a main driver for TC variability. The existence of such a correlation is proven in their study and its existence is not argued here. However, correlation does not imply causation and the use of cyclogenesis indices support the idea that the decrease of mid-tropospheric humidity, not the decrease of vorticity, may be the dominant driving mechanism involved in TC decrease over Australia.

4 Discussion and conclusions

In this study, we have attempted to compare the annual mean and seasonal to interannual variability of four cyclogenesis indices: the GPI, CYGP, YGP and TCS

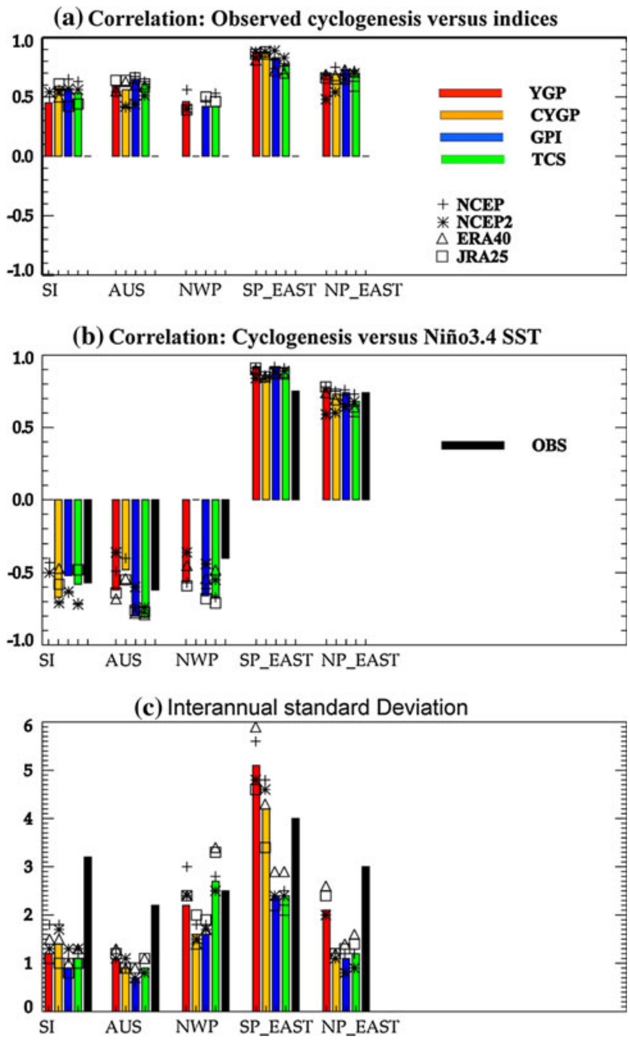

Fig. 14 Same as Fig. 10 but for the *boxes* of Fig. 12

(Tippett et al. 2011) for the period 1979–2001. We have also tested how the index performances vary with the four reanalyses ERA40, NCEP, NCEP2 and JRA25. There are usually more differences between indices for a given forcing than between one index calculated using different reanalyses. Considering the climatology, one obvious flaw of the YGP, GYGP and GPI is a ~2.5°–5° equatorward bias of the main cyclogenesis areas, especially visible in the northern hemisphere. This bias does not exist in the TCS index where the use of a "clipped" vorticity is the key for suppressing such offset (Tippett et al. 2011). The spatial distributions of the biases are not homogeneous with regions of positive and negative biases. Errors in the mean numbers can reach up to 50% positively or negatively in large regions.

On seasonal timescales, another flaw found in all indices—although to a lesser extent in the TCS—is the overestimation of simulated cyclogenesis during unfavourable seasons. The index response variety in different regions also renders making a general conclusion difficult. Again, the mechanisms explaining the seasonal variations as deduced from individual terms that compose the indices do, in fact, differ from one index to another significantly. This result leads us to advise caution when deducing specific mechanisms from (only) one index as is sometimes done (e.g. Yokoi et al. 2009). Overall, however, we feel that the TCS is perhaps the best-adjusted index on seasonal timescales.

When examining the interannual scales, we have distinguished the effect of ENSO from the interannual variability. In general, the indices do not accurately represent the observed interannual cyclogenesis as significant regional correlation rarely exceeds 0.6 on annual averages. Furthermore, all the indices strikingly underestimate the observed amplitudes almost everywhere and when they do not, their correlation to observations is often weak or insignificant on sub-basin scales. However, it seems evident that estimating index performances on large regions blurs their performances because sub-regional patterns may vary oppositely within one large region. These sub regional variations are usually linked to ENSO.

ENSO is a major contributor to interannual genesis. It usually induces patterns of dipole anomalies where enhanced cyclogenesis lies next to weakened cyclogenesis. Thus, a sub regional analysis on areas of coherent ENSO impact is preferable. Unlike our previous conclusions, cyclogenesis phase changes linked to ENSO are coherently simulated by the indices and compare acceptably with observations on most occasions. However, correlation of indices to ENSO is often higher than correlation of actual cyclogenesis to ENSO. This suggests that the indices overestimate the actual cyclogenesis variability responding to ENSO. The indices still usually exhibit large discrepancies to observations on ENSO timescales in terms of variability amplitude even in regions like the South Pacific Convergence Zone where interannual correlation to ENSO can reach 0.8 both in observations and in the indices.

When considering the mechanisms (thermal and dynamical terms) explaining the distributions, we have shown that they can differ significantly between indices at all timescales (except ENSO), which renders the understanding of the individual mechanisms involved in actual cyclogenesis somewhat speculative. This is especially true when using a single index (e.g. Yokoi et al. 2009). On most occasions, there has been a failure to understand the main faults leading to obvious misrepresentation of cyclogenesis variations in specific basins and specific indices. This is mostly due to the complexity of interplay between the individual terms for each index. Another reason is because the overall index performances vary from basin to basin. However, all the indices basically agree on the mechanisms controlling ENSO-related cyclogenesis variations,

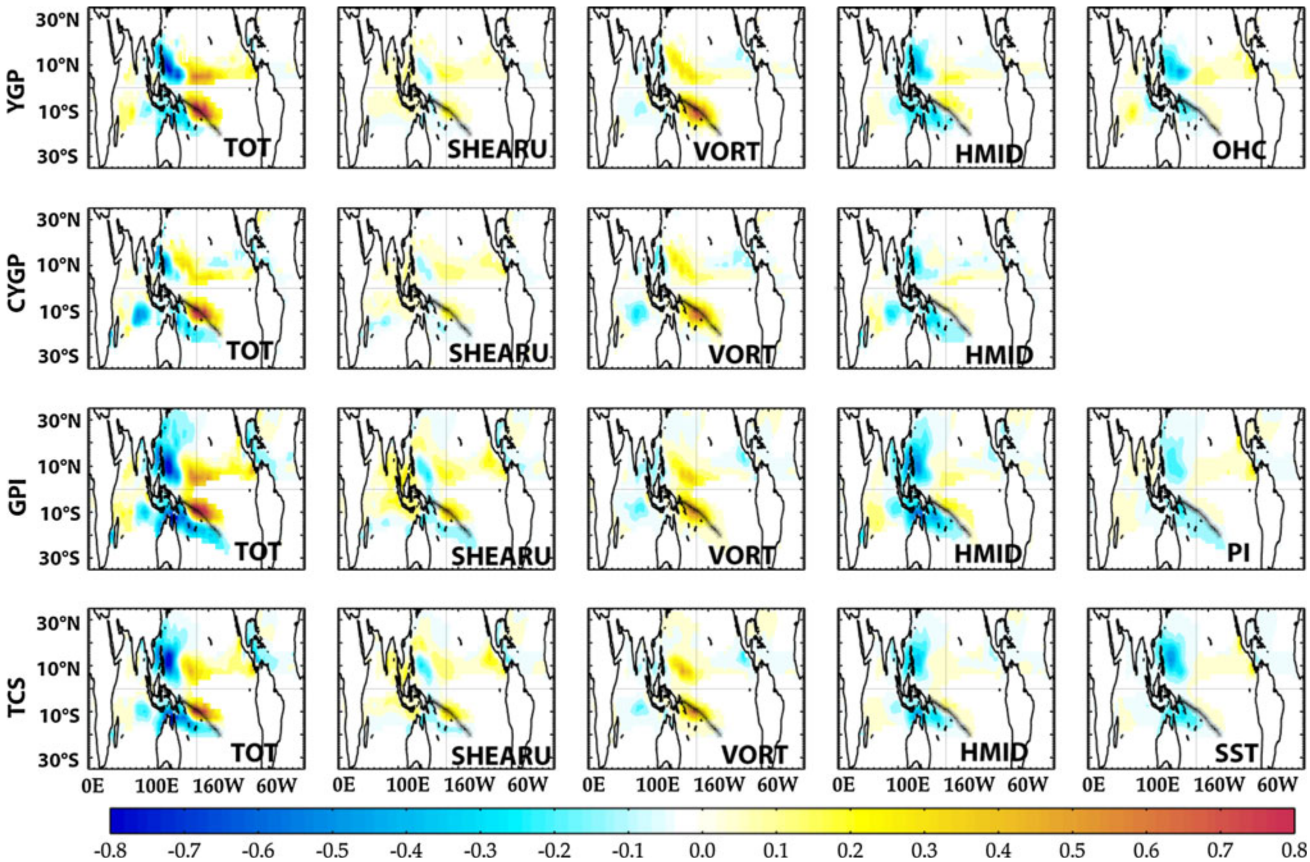

Fig. 15 Standardized regressions of selected (dominant) terms on the ENSO index. Note that the first column is the regression of the total index to the ENSO index, the second is the regression of the wind shear to ENSO, third is the regression of vorticity term to the ENSO index; fourth is the humidity term and fifth is the ocean heat term for the YGP, potential intensity for the GPI, and SST index for the TCS

suggesting that the conclusions reached on the basis of a single index are valid.

The global discrepancies found in the mean, seasonal and interannual amplitudes simulated by all the indices cannot be corrected by the simple use of a global constant that fits the mean yearly-observed cyclogenesis. Kim et al. (2010) discuss this point and conclude that it may be better to use regionally adjusted constants even if their justification would remain unclear. We have tried to apply such spatially dependent correction by fitting the mean indices to observations at each point. While the use of such *ad hoc* correction improves the seasonal variations, it has globally no effect on reducing the biases found in the interannual variations. Eventually, we believe that regional improvements can only come from a new adjustment of the functional forms or of the type of variable entering the index. Along these lines, Murakami and Wang (2010) have added a new term to the GPI to improve the index performances in the northwestern Pacific. Similarly, Emanuel (2010) has proposed a modified version of the GPI, which seems to be more suited for climate projections. The analyses conducted in the present study, although not exhaustive, present a benchmark with which to test these new indices and other future indices.

The question arises as to what extent genesis indices can be expected to reproduce observed cyclogenesis. These indices are only indications of the large-scale conditions favourable to cyclogenesis. Hence, while large-scale conditions may be favourable, actual cyclogenesis may not necessarily occur. This may explain why indices can be better correlated to ENSO than to actual cyclogenesis. One important mechanism controlling cyclogenesis in a favourable environment relies on stochastic processes. These are not represented by the indices but have been shown to be potentially important for cyclogenesis (Simpson et al. 1997). For example, Jourdain et al. (2010) have specifically shown using a high resolution model of the SPCZ region that roughly half of the South Pacific cyclogenesis may be due to stochasticity while the large-scale forcing represented by the indices explains the remaining variability. This may also explain why the global high-resolution simulations of Zhao et al. (2009) poorly simulate the variability of the South Pacific region (see their Fig. 11a) while the North Atlantic variability is much better simulated. It is interesting to note that Camargo et al. (2009) invoke a similar argument to explain some discrepancies between the GPI and the observations at MJO timescales.

Compared to large-scale forcing that may be predictable, especially if dominated by ENSO, stochasticity limits predictability of cyclogenesis on intraseasonal to interannual timescales. Stochasticity has, however, no effect on long-term estimations. Yet, given the large regional biases of climatological indices and the failure of GCMs to capture a number of observed atmospheric trends (Emanuel 2010), the evaluation of the long-term regional cyclogenesis changes associated with climate change using these indices (Caron and Jones 2008; Royer and Chauvin 2009; Chauvin and Royer 2011; Kim et al. 2010) remains an issue to be addressed with caution., Finally, in this study, no attempt was made to compare the interannual variability of the indices within the framework of climate models such as those used in the IPCC-AR4 database. Given the divergence of our results to observations, and the vast diversity of ENSO response in these models (Collins et al. 2010), we believe that the indices are not equipped to give quantitative regional estimates of interannual cyclogenesis in the future climate. This should be addressed more precisely in future work.

Acknowledgments The authors wish to thank K. Emanuel for sharing the cyclone netcdf data as well as the GPI routines. We would like to thank our two anonymous reviewers for their fruitful comments. Thanks also goes to Michael Tippett for insightful discussions and for sharing his results prior to publication. This work was supported by the Institut de Recherche pour le Développement (IRD) and ANR grant ANR-VULN-002-01. The JRA25 datasets are from the JRA-25 long-term reanalysis cooperative research project carried out by the JMA and the CRIEPI.

Appendix: cyclogenesis index definition

In the text, we use the label "reanalysis-index" (e.g., NCEP-YGP, ERA40-GPI etc…) for an index calculated with a given reanalysis. The definitions that follow are exact replications of those found in the original papers. They are:-

1. GPI

The GPI monthly index is constructed as in Camargo et al. (Camargo et al. 2007a, b) and Emanuel and Nolan (2004) as $\mathrm{GPI} = \underbrace{\left|10^5\eta\right|^{3/2}(1+0.1V_{\mathrm{shear}})^{-2}}_{\text{dynamic}} \underbrace{\left(\frac{H}{50}\right)^3\left(\frac{V_{\mathrm{pot}}}{70}\right)^3}_{\text{thermal}}$

with η is the absolute vorticity at 850 hPa in s^{-1}, H is the relative humidity at 600 hPa, V_{pot} is the potential intensity calculated using a routine provided by Dr. Emanuel (http://wind.mit.edu/~emanuel/home.html). V_{shear} is the magnitude of the vertical wind shear between 850 and 200 hPa in ms^{-1}. For consistency with the other indices below, we sometimes refer to thermal and dynamical potentials (see equation).

2. TCS (Tippett et al. 2011)

This index uses the same variables as the previous one except for the V_{pot} which is replaced by an SST index:

$$\begin{aligned}\mathrm{TCS} &= \exp(b + b_\eta\eta + b_{V_{\mathrm{shear}}}V_{\mathrm{shear}} + b_H H + b_T T + \log(\cos\phi)) \\ &= \cos\phi * \exp b * \underbrace{\exp(b_\eta\eta + b_{V_{\mathrm{shear}}}V_{\mathrm{shear}})}_{\text{dynamic}} * \underbrace{\exp(b_H H + b_T T)}_{\text{thermal}},\end{aligned}$$

with $T = \mathrm{SST} - \overline{\mathrm{SST}}^{[20°\mathrm{S}-20°\mathrm{N}]}$ and $\eta = \min(\eta, 3.7)$ is referred to as the "clipped vorticity", φ is the latitude. The constant used in the calculation is that given by Tippett et al. (2011)'s Table 1 line 6, namely: $b = 5.8$; $b_\eta = 1.03$; $b_H = 0.05$; $b_T = 0.56$; $b_V = -0.15$.

3. YGP

For consistency with the GPI, we have constructed monthly YGP and CYGP indices rather than seasonal indices as initially proposed by Gray (1979), Watterson et al. (1995), Royer et al. (1998). The monthly YGP is calculated as $\mathrm{YGP} = \underbrace{|f|I_\zeta I_s}_{\text{dynamic}}\underbrace{EI_\theta I_{\mathrm{RH}}}_{\text{thermal}}$ where f is the Coriolis parameter in $10^{-5}\mathrm{s}^{-1}$, $I_\zeta = \zeta_r\frac{f}{|f|} + 5$ with ζ_r the relative vorticity at 925 hPa in $10^{-6}\ \mathrm{s}^{-1}$, $I_s = \left(\left|\frac{\delta V}{\delta P}\right| + 3\right)^{-1}$ where $\frac{\delta V}{\delta P}$ is the vertical shear of the horizontal wind between 925 and 200 hPa in m s^{-1}/750 hPa, $I_\theta = \left(\frac{\delta\theta_e}{\delta P} + 5\right)$ where $\frac{\delta\theta_e}{\delta P}$ is the vertical gradient of the equivalent potential temperature between 925 and 500 hPa in K/500 hPa, $I_{\mathrm{RH}} = \max\left(\min\left(\frac{\mathrm{RH}-40}{30}, 1\right), 0\right)$ with RH is the average relative humidity in percent between 700 and 500 hPa. More simply put, if RH is greater than 70% then $I_{\mathrm{RH}} = 1$ and if RH lower than 40%, $I_{\mathrm{RH}} = 0$. $E = \int_0^{60m}\rho_w c_w(T-26)dz$ is the thermal energy of water above 26°C in the top 60 m of the ocean. ρ_w and c_w are the density and specific ocean heat capacity taken as constant. We have access to two OGCMs (Ocean General Circulation Model) outputs forced by NCEP and ERA40 reanalyses from the OPA model (Rodgers et al. 2008) with which to calculate E but we do not have similar outputs for the NCEP2 reanalyses. However, the averaged E over 25°S–25°N, 0–360° and for the 1970–2001 time period yields 7.6 10^3 cal cm^{-2} for NCEP-OPA (referring to the OPA output forced by NCEP) and 7.9 for ERA40-OPA outputs. The two time series correlate at 0.98 and their respective standard deviation are 0.92 and 0.99. Thus, despite differences in the two wind fields, the OGCM thermal energy E yields very similar quantities. Hence, it is reasonable to think that NCEP2-OPA, if it existed, would have also given a very similar E. Thus, we have confidently used E from NCEP-OPA in the calculation of the NCEP2 YGP.

4. CYGP

The CYGP replaces the thermal potential of the YGP by a convective potential $k(P_c - P_0)$where k is an arbitrary constant to be adjusted depending on the reanalysis or data set used. P_c is the convective precipitation in mm day^{-1} and P_0 is a threshold below which the convective potential is set to zero to avoid spurious cyclogenesis off the tropics. We chose $P_0 = 3$ from previous studies (Chauvin and Royer 2011; Royer and Chauvin 2009) but tests on this threshold do not change the analyses performed in that paper. k was adjusted for each reanalysis in order to yield a $\sim$85 cyclone/year global mean, as observed (see also main text).

For consistency with the GPI, we have constructed monthly YGP and CYGP indices rather than seasonal indices as initially proposed by Gray (1979), Watterson et al. (1995), Royer et al. (1998). It was checked that introducing monthly variations rather than 3-month seasons does not induce significant differences in the seasonal index estimates.

References

Bruyere C, Holland G, Done J, Suzuki-Parker A (2010) Genesis potential index for tropical cyclones in the nested regional climate model (NRCM) experiments. In: Proceedings of 29th conference on hurricanes and tropical meteorology, Tucson, Arizona, 10–14 May 2010, 7A.2

Camargo SJ, Sobel AH (2007) Workshop on tropical cyclones and climate. Bull Metorol Soc 88(3):389–391. doi:10.1175/BAMS-88-3-389

Camargo SJ, Emanuel KA, Sobel AH (2007a) Use of a genesis potential index to diagnose ENSO effects on tropical cyclone genesis. J Clim 20:4819–4834

Camargo SJ, Sobel AH, Barnston AG, Emanuel KA (2007b) Tropical cyclone genesis potential index in climate models. Tellus 59A:428–443

Camargo SJ, Wheeler MC, Sobel AH (2009) Diagnosis of the MJO modulation of tropical cyclogenesis using an empirical index. J Atmos Sci 66:3061–3074

Caron LP, Jones CG (2008) Analysing present, past and future tropical cyclone activity as inferred from an ensemble of coupled global climate models. Tellus 60A:80–96

Chand SS, Walsh KJE (2009) Tropical cyclone activity in the Fiji region: spatial patterns and relationship to large-scale circulation. J Clim 22:3877–3893

Chauvin F, Royer J-F (2011) Role of the SST anomaly structures in response of cyclogenesis to global warming. In: Elsner JB et al (eds) Hurricanes and climate change, vol 2. Springer Science, Berlin. doi:10.1007/978-90-481-9510-7_3

Chauvin F, Royer J-F, Déqué M (2006) Response of hurricane-type vortices to global warming as simulated by ARPEGE-Climat at high resolution. Clim Dyn 27:377–399

Chu PS (2004) ENSO and tropical cyclone activity. In: Murnane RJ, Liu K-B (eds) Hurricanes and typhoons, past, present and future. Columbia University Press, Columbia, pp 297–332

Collins M, An S-I, Cai W, Ganachaud A, Guilyardi E, Jin F-F, Jochum M, Lengaigne M, Power S, Timmermann A, Vecchi G, Wittenberg A (2010) The impact of global warming on the tropical Pacific and El Niño. Nat Geosci 3:391–397. doi:10.1038/ngeo868

Emanuel K (2010) Tropical cyclone activity downscaled from NOAA-CIRES reanalysis, 1908–1958. J Adv Model Earth Syst 2:1–12. doi:10.3894/JAMES.2010.2.1

Emanuel KA, Nolan DS (2004) Tropical cyclone activity and global climate. In: Proceedings of 26th conference on hurricanes and tropical meteorology. American Meteorological Society, Miami, FL, pp 240–241

Gray WM (1968) Global view of the origin of tropical disturbances and storms. Mon Weather Rev 96:669–700

Gray WM (1975) Tropical cyclone genesis. Colorado State University, Colorado

Gray WM (1979). Hurricanes: their formation, structure and likely role in the tropical circulation. Meteorology over the Tropical Oceans. Ed R Meteor Soc 155–218

Gray WM (1998) The formation of tropical cyclones. Meteorol Atmos Phys 67:37–69. doi:10.1007/BF01277501

Grotjahn R (2008) A comparison of selected fields in NCEP/DOE AMIP-II and ECMWF ERA-40 reanalyses. Dyn Ocean Atmos 44:108–142

Jourdain NC, Marchesiello P, Menkes CE, Lefèvre J, Vincent EM, Lengaigne M and Chauvin F (2010) Mesoscale simulation of tropical cyclones in the South Pacific: climatology and interannual variability. J Clim. doi: 10.1175/2010JCLI3559.1

Kalnay EC et al (1996) The NCEP/NCAR reanalysis project. Bull Am Meteorol Soc 77:437–471

Kanamitsu M, Ebisuzaki W, Woollen J, Yang S-K, Hnilo JJ, Fiorino M, Potter GL (2002) NCEP-DOE AMIP-II reanalysis (R-2). Bull Am Meteor Soc 83:1631–1643

Kim J-H, Brown S, McDonald RE (2010) Future changes in tropical cyclone genesis in fully dynamic ocean- and mixed layer ocean-coupled climate models: a low-resolution model study. Clim Dyn. doi:10.1007/s00382-010-0855-6

Kim HM, Webster PJ, Curry JA (2009) Impact of shifting patterns of Pacific Ocean warming on North Atlantic tropical cyclones. Science 325:77–80. doi:10.1126/science.1174062

Landsea CW (2000) El Niño–Southern oscillation and the seasonal predictability of tropical cyclones. In: Díaz HF, Markgraf V (eds) El Niño: impacts of multiscale variability on natural ecosystems and society. Cambridge University Press, Cambridge, pp 149–181

Lyon B, Camargo SJ (2009) The seasonally-varying influence of ENSO on rainfall and tropical cyclone activity in the Philippines. Clim Dyn 32:125–141. doi:10.1007/s00382-008-0380-z

McDonald RE, Bleaken DG, Cresswell DR, Pope VD, Senior CA (2005) Tropical storms: representation and diagnosis in climate models and the impacts of climate change. Clim Dyn 25:19–36

Murakami H, Wang B (2010) Future change of North Atlantic tropical cyclone tracks: projection by a 20-km-mesh global atmospheric model. J Clim 23:2699–2721

Onogi K, Tsutsui J, Koide H, Sakamoto M, Kobayashi S, Hatsushika H, Matsumoto T, Yamazaki N, Kamahori H, Takahashi K, Kadokura S, Wada K, Kato K, Oyama R, Ose T, Mannoji N, Taira R (2007) The JRA-25 reanalysis. J Meteorol Soc Jpn 85:369–432. doi:10.2151/jmsj.85.369

Ramsay HA, Leslie LM, Lamb PJ, Richman MB, Leplastrier M (2008) Interannual variability of tropical cyclones in the Australian region: role of large-scale environment. J Clim 21:1083–1103. doi:10.1175/2007JCLI1970.1

Rodgers KB, Aumont O, Menkès C, Gorgues T (2008) Decadal variations in equatorial Pacific ecosystems and ferrocline/pycnocline decoupling. Glob Biogeochem Cycles 22(2):17–32

Royer J-F, Chauvin F (2009) Response of tropical cyclogenesis to global warming in an IPCC AR-4 scenario assessed by a modified yearly genesis parameter. In: Elsner JB, Jagger TH (eds) Hurricanes and climate change. Springer, Berlin, pp 213–234

Royer J-F, Chauvin F, Timbal B, Araspin P, Grimal D (1998) A GCM study of the impact of greenhouse gas increase on the frequency of occurrence of tropical cyclones. Clim Chang 38:307–343

Simpson J, Ritchie E, Holland G, Halverson J, Stewart S (1997) Mesoscale interactions in tropical cyclone genesis. Mon Weather Rev 125(10):2643–2661

Tippett MK, Camargo SJ, Sobel A (2011) A poisson regression index for tropical cyclone genesis and the role of large-scale vorticity in genesis. J clim. doi:10.1175/2010JCLI3811.1, accepted

Trenberth KE (1997) The Definition of El Niño. Bull Am Meteorol Soc 78:2771–2777

Tsutsui JI, Kasahara A (1996) Simulated tropical cyclones using the National center for atmospheric research community climate model. J Geophys Res Atmos 101:15013–15032

Uppala SM, Co-authors (2005) The ERA-40 re-analysis. Q J R Meteorol Soc 131(612 Part B):2961–3012

Vincent E, Lengaigne M, Menkes CE, Jourdain NC, Marchesiello P, Madec G (2009) Interannual variability of the South Pacific convergence zone and implications for tropical cyclone genesis. Clim Dyn. doi:10.1007/s00382-009-0716-3

Watterson IG, Evans JL, Ryan BF (1995) Seasonal and interannual variability of tropical cyclogenesis: diagnostics from large-scale fields. J Clim 8:3052–3066

Yokoi S, Takayabu YN, Chan JCL (2009) Tropical cyclone genesis frequency over the western North Pacific simulated in medium-resolution coupled general circulation models. Clim Dyn 33:665–683. doi:10.1007/s00382-009-0593-9

Zhao M, Held IM, Lin S-J, Vecchi GA (2009) Simulations of global hurricane climatology, interannual variability, and response to global warming using a 50 km resolution GCM. J Clim. doi: 10.1175/2009JCLI3049.1